



Investigation of Urban Heat Islands and modeling of Land Surface Temperature over selected Indian cities using MODIS products

Nirup Sundar Mandal¹ · Kironmala Chanda^{1,2}

Received: 18 February 2025 / Accepted: 13 April 2025 / Published online: 25 April 2025
© The Author(s), under exclusive licence to Springer-Verlag GmbH Austria, part of Springer Nature 2025

Abstract

Investigation on Land Surface Temperature (LST) and Urban Heat Island (UHI) is essential for cities at various stages of urban development, which is often overlooked. This study examines the UHI effect at selected Tier 2 cities in India with varying size and developmental stages. MODIS products such as MOD11A1, MOD09A1 and MCD12Q1 for the duration 2006–2022 were used for computing various spectral indices along with corresponding Land Use Land Cover (LULC) and LST. Results indicated that the highest UHI effect (above 3 °C) was experienced in Gurgaon (heavily built-up, scarce vegetation within core urban area) during summer nights. Small, unplanned cities like Dahegam and Kalol in Gandhinagar district experienced higher LST and UHI effect than the nearby planned state capital, Gandhinagar. On the other hand, the small, refinery city of Bongaigaon indicated Urban Cool Island (UCI) effect even during summers, due to the presence of vegetation within its core urban area. The potential of two network based algorithms – Convolutional Neural Networks (CNN) and Recurrent Neural Networks (RNN) in modelling LST using the MODIS derived spectral indices and LULC classes as inputs is compared. Both CNN/RNN modelled LST showed good agreement with observations with R^2 values during model testing period as high as 0.940/0.997 for Gandhinagar District, 0.991/0.996 for Bongaigaon and 0.988/0.993 for Gurgaon Administrative Division. The analysis of LST variation and seasonal UHI effects may be a key to the development of sustainable communities not only in large cities but also the less investigated smaller cities with similar concern.

Keywords Urban heat island · Land use land cover · Spectral indices · Land surface temperature · Convolutional neural network · Recurrent neural network

1 Introduction

Urban planning and development by Government agencies is often plagued with severe sustainability dilemmas. The Sustainable Development Goal (SDG) #11 of the United Nations has a consideration for sustainable human settlement planning and management in all countries by incorporating resource efficiency, proper mitigation and adaptation to climate change. In recent times, the growth of urban areas with dense construction have triggered higher temperatures in the core urban areas when compared to the surrounding non-urban areas. This difference in temperature, where

urban cities experience a comparatively higher temperatures than surrounding non-urban areas, is known as the Urban Heat Island (UHI)(Wong and Yu 2005; Zhou et al. 2013). The concept was first identified and studied by Luke Howard while researching urban climate in London, England, as noted by Yang et al. (2016). The level of reflection, or albedo, plays quite a significant role for UHI. Areas with higher albedo will reflect more sunlight, resulting in higher Land Surface Temperatures (LST), according to Zhou et al. (2013) and Varamesh et al. (2022). Built-up areas generally have higher albedo values than any other natural covers thus contributing to increased reflection, as highlighted by Schlaerth et al. (2023). Additionally, barren lands also possess relatively high albedo levels (Varamesh et al. 2022). Besides these natural occurrences, various studies indicate that human activities can further exacerbate the intensity of UHI in densely populated cities. Factors such as heat emissions from vehicles, buildings, and even human metabolism contribute to the elevated temperatures within urban areas

✉ Kironmala Chanda
kironmala@iitism.ac.in

¹ Department of Civil Engineering, Indian Institute of Technology (Indian School of Mines), Dhanbad, India

² Centre for Water Resources Management, Indian Institute of Technology (Indian School of Mines), Dhanbad, India

and reinforce heat extremes within a city (Zhou et al. 2013; Liu et al. 2021). With the development of technical know-how and increased need of urban facilities, many major Indian cities have evidenced unplanned urban growth. For instance, there are several developing cities in Assam; however; an absence of proper road density and networks has led to poor connectivity to remote areas in the state which impedes development from natural potentialities like vegetation, minerals, agriculture etc. (Konwar 2024). A temporal study on the capital of Assam, Guwahati confirmed that the city is on the verge of urban sprawl and thus inviting UHI conditions (Borah and Sarma 2025). Decrease of vegetation and increase of urban area in Cuttack, Odisha has led to a rise in LST by 6.6 °C within three decades (Patra et al. 2025). Meerut, a city in Uttar Pradesh near New Delhi, is also gearing up for major urban expansion with several upcoming development projects. While this growth brings new opportunities, it also raises concerns about heat stress, traffic congestion, rising energy consumption, and worsening air pollution (Joshi et al. 2025). LST is related to aerosols inversely; Gohain et al. (2023) have found that Indore reports high aerosol values in summers and low aerosol values in winters; thus, leading to an increasing trend of LST in summers and decreasing trend of LST in winters. The decreasing LST in core urban areas may lead to the development of Urban Cool Islands (UCI). An UCI study by Sarif et al. (2022) based on Bengaluru recommends that vegetation and water bodies can aid thermal stability in megacities.

Previous researches show that Land Surface Temperature (LST) is negatively correlated to the Normalized Difference Vegetation Index (NDVI) during warm seasons and positively correlated in winters (Sun and Kafatos 2007; Guha and Govil 2021; Almouctar et al. 2024). By looking at multi-temporal images, one can evidence the LST changes with NDVI (Tan et al. 2012; Raza et al. 2024) despite the impact of seasons. On a different note, LST has a positive correlation with the Normalized Difference Built-up Index (NDBI) and the highest correlations are observed in built-up areas mostly (Subzar Malik et al. 2019; Alademomi et al. 2022). Transforming green areas into urban spaces has led to higher LST levels in various parts of the globe (Khamchiangta and Dhakal 2020; Mohammad Harmay et al. 2021). The positive link between LST and NDBI highlights how developed regions can enhance the Urban Heat Island effect (Kaplan et al. 2018). Typically, most studies have indicated that LST and NDBI follow a consistent linear trend and have a strong to moderate correlation throughout all seasons (Zeng et al. 2010; Guha and Govil 2022). This makes NDBI a preferred index for exploring its relationship with LST since it's not influenced by climate conditions, unlike NDVI which is climate-dependent (Shahfahad et al. 2020). Although the connection between LST and NDBI may vary occasionally based on seasons, this is usually limited to specific cases

(Mathew et al. 2017). Additionally, LST shows a negative correlation with the Modified Normalized Difference Water Index (MNDWI) but a positive correlation with the Normalized Difference Bareness Index (NDBaI) (Sun et al. 2013; Khan et al. 2024). Linear modeling has verified such relationships between LST and NDVI, NDBI, as well as the Normalized Difference Water Index (NDWI)(Feng et al. 2018). Areas with water bodies tend to have lower LST compared to dry landscapes like built-up and barren land (Santhosh and Shilpa 2023; Joshi et al. 2025). Also, larger and well-shaped water bodies are effective in reducing temperatures (Jandaghian and Colombo 2024).

UHI effect is a pressing contemporary issue that stands to worsen in the future due to climate change. Predicting the future LST of urban areas has become increasingly crucial in recent years. Machine Learning (ML) models are found to perform soundly for such future projections (Bochenek and Ustrnul 2022). In a study conducted by Uddin and Lu (2024), it was clear that tree-based ML algorithms performed significantly better as compared to non-tree-based algorithms for image studies. Several studies have highlighted that ML models possess the capability to predict LST. Mohammad and Goswami (2021) have demonstrated the effectiveness of Multiple Linear Regression (MLR) and ANN in LST prediction. Equere et al. (2021) used ANN to predict UHII spatial distribution, emphasizing the significance of Terrain Factor (TF) over NDVI or NDBI. By utilizing predictors like NDVI, NDBI, and Elevation Factor (EF), Equere et al. (2021) derived a predictive model for LST. Kartal and Sekertekin (2022) incorporated spatial interpolation techniques and Deep Learning methods to obtain spatiotemporal LST predictions. Furthermore, accurate projection of future land cover is essential for projecting LST based on land cover information. The Classification and Regression Tree (CART) algorithm has successfully forecasted changes in Land Use Land Cover (LULC) and LST trends over time (Muhammad et al. 2022). They also used machine learning methods like XGBoost, Support Vectors and Random Forests for LST prediction. Support Vector Machines (SVM), coupled with suitable model builders, have been used to generate seasonal LST Maps reflecting significant increases in LST variations contributing to the Surface Urban Heat Island phenomenon (Kafy et al. 2021). They developed a Cellular Automata based Artificial Neural Network model for predicting potential LULC, LST, and Urban Thermal Field Variance Index trends. Zhang et al. (2023) introduced the Improved Whale Optimized Algorithm – Long Short-Term Memory model to project future summer and winter LST trends, highlighting an expanding high-temperature urban area diminishing urban comfort levels. Additionally, Tan et al. (2012) employed Convolutional Neural Networks for microwave radiation transmission simulation, revealing minor winter surface temperature changes in specific regions

and spatial-temporal Siamese convolutional neural network (SSCNN) can be used to reconstruct Subsurface Temperature data (Zhang et al. 2024). Moreover, Liu et al. (2022) found Extreme Gradient Boosting beneficial for correcting biases in daily LST estimation during automatic observations – thereby averting overestimation of LST temperatures.

It is noted that investigation on LST and UHI is essential in the current era of climate change and the need for developing sustainable cities and communities. However, in the existing literature, UHI studies are mostly concentrated over large cities and there is a lack of studies on smaller cities, particularly in India. Moreover, there is inadequacy in modeling studies which capture the association of LULC and LST; such modeling is possible in recent times with the availability of high-resolution satellite images and products and will be attempted in this study. Further, the potential of neural network-based ML approaches in capturing such association has not been explored thoroughly in existing literature. Hence, this study has two main objectives: (i) to examine the UHI/UCI effect across selected regions in India with various climatic types and stages of urban development utilizing fine resolution MODIS satellite products (ii) to explore the potential of neural network based ML approaches in modeling LST utilizing satellite based spectral indices and LULC information as inputs. This study examines five Indian cities, analysing the occurrence of UHI/UCI while also exploring their variations in relation to LULC. The findings can help city planners understand the causes of these phenomena and develop policies to mitigate their impact.

2 Materials and methods

2.1 Study area

The study was conducted on three different regions across India having various climatic types—Gandhinagar of Gujarat, Bongaigaon of Assam and Gurgaon of Haryana. Gandhinagar and Gurgaon are rapidly developing large Indian cities whereas Bongaigaon is a much smaller refinery city. In addition to Gandhinagar, two small neighbouring towns—Kalol and Dahegam, were also investigated upon observing UHI effect in them. To assess the UHI effect of all the above-mentioned tier- 2 cities of India, the considered study area consisted of the city and the surrounding non-urban region, including the majority of the district. Figure 1 shows the map of India with all the considered study regions, and the following paragraphs provide a description of the study areas.

Gandhinagar (23.22° N, 72.64° E) is located in the western part of the country and is the capital city of Gujarat state. As per the Koppen Climate Classification, Gandhinagar falls

under the mid-latitude steppe and desert climate category. Located on the banks of River Sabarmati at an altitude of 81 m, the city spans over an area of 326 km^2 and has recorded a highest temperature of 48.0° C in 2016 and a lowest temperature of 4.3° C in the year 2021. The city experiences three main seasons: summer, monsoon and winter. The months of March, April, May and June are very hot and thus constitute the summer season, whereas December to January makes the winter season. The climate is dry in both seasons but becomes humid from mid-June to mid-September upon arrival of the southwest monsoon. The considered study region included Gandhinagar and the major part of the district making up an area of 6076.72 sq. km.

Dahegam (23.17° N, 72.82° E) is located in Gandhinagar district about 25 km to the east of the capital city Gandhinagar and has an average elevation of 73 m. The city has an area of 27 km^2 and very scarce amount of greenery and its temperature comparable to Gandhinagar.

Located between the towns of Mehsana and Ahmedabad on Gujarat State Highway 41, Kalol (23.25° N, 72.50° E) is another smaller city in the Gandhinagar district of Gujarat, India. With an area of 25.2 km^2 , it has an elevation of 81 m. Inspite of being a small city, it has been a hub of industrial development which is one of the major driving factor for urban growth and sprawl (Purwani et al. 2022). The climate is dry. From mid-June until mid-September, the southwest monsoon brings with it a humid climate. About 803.4 mm of rain falls on average each year. From March to June, the temperature ranges from 35 to 49° C at its maximum and 12 to 26° C at its minimum, making it hot to extremely hot. Kalol's highest recorded temperature was 49.8° C in May 2019. December through February experience an average high temperature of about 26° C and an average lowest temperature of 12° C.

Bongaigaon is one of the major oil refinery cities located in the western part of the North-Eastern Indian state of Assam (26.50° N, 90.55° E) and serves as a gateway to the North Eastern Frontier Railway Zone. Located 200 km to the west of the state capital, Guwahati, Bongaigaon is situated 62.6 m above sea level. The city has been a facility to oil exploration and the presence of an oil refinery has led to the growth of the city (Bahadur 2009). The city has a humid climate, which is very much influenced by the monsoon, and it experiences a sub-tropical climate as per the Koppen Climate Classification. Summers are not very hot, accounting for the highest temperature of 38.9° C to date in 2022, whereas the lowest recorded is 8° C, indicating a mild cold winter. This is mostly due to the vegetation patches within the city, which has a high NDVI value. Being a small city, the considered study area (including the neighbouring non-urban area) summated around 967.20 sq. km.

Gurgaon, or Gurugram, is a satellite city of the Indian capital, New Delhi and hence belongs to the northern part

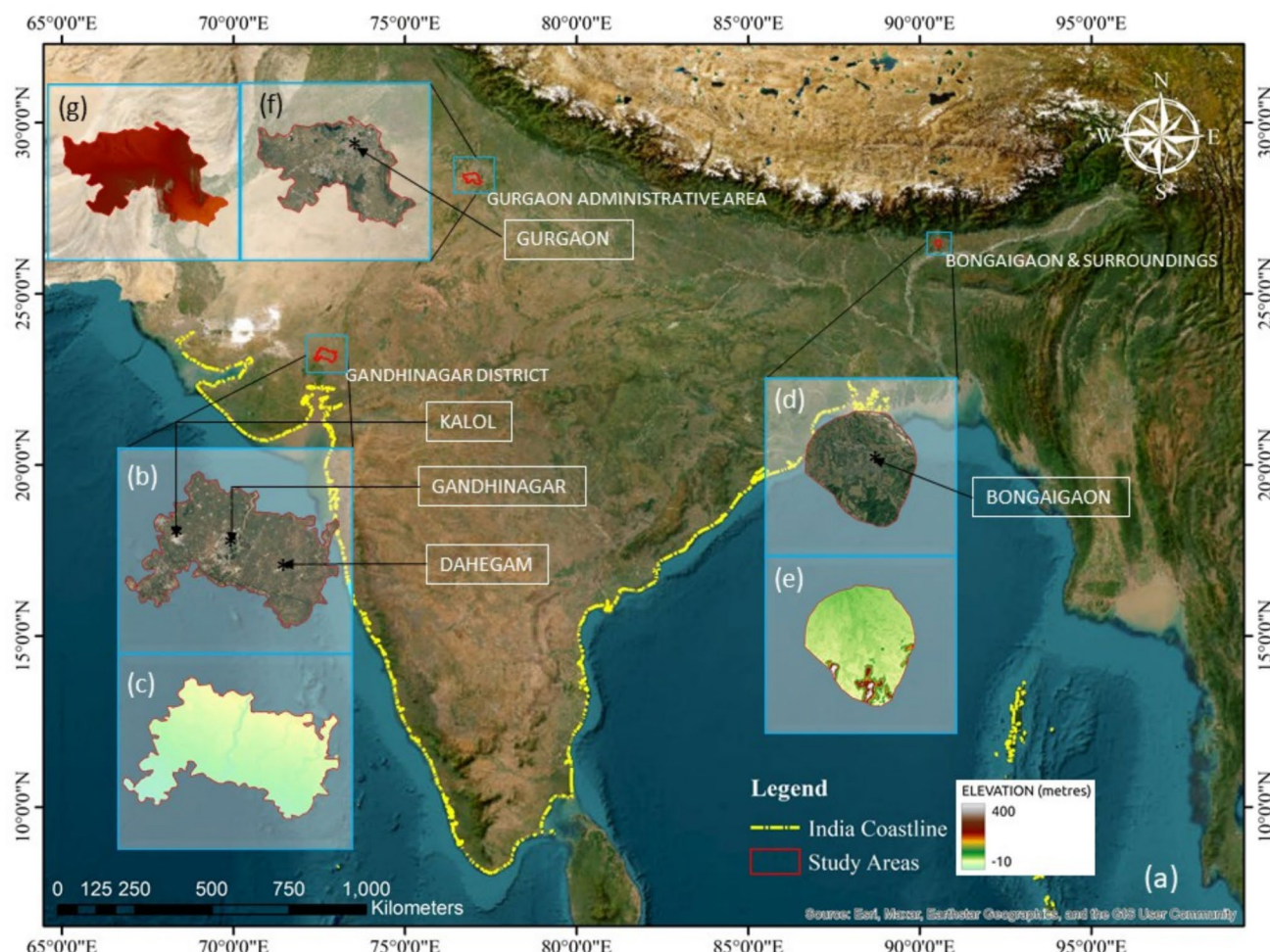


Fig. 1 (a) Location of study areas in India in satellite imagery; (b) satellite imagery of Gandhinagar district, (c) digital elevation model (DEM) map of Gandhinagar district, (d) satellite imagery of Bongaigaon and surroundings, (e) DEM map of Bongaigaon and sur-

roundings, (f) satellite imagery of Gurgaon administrative area and (g) DEM map of Gurgaon administrative area (Source: Esri, Maxar, Earthstar Geographics, and the GIS user community and shuttle radar topography mission DEM)

of the country. It is situated at the Delhi-Haryana border and belongs to Haryana state and is situated 30 km southwest of New Delhi and 268 km south of the state capital of Chandigarh. The coordinates are 28.46° N, 77.03° E. Jain et al. (2017) have showed the growth of urbanization in Gurgaon by over 10% from 1995 to 2015. The city has an overlap of monsoon-influenced humid subtropical climate and a hot semi-arid climate as per the Koppen Climate Classification. The city spans around 232 km^2 and is India's second-largest information technology hub and third-largest financial and banking hub. The highly built-up areas typically contribute to a hot and humid climate during the summers (March-August), recording a maximum temperature of 48.1°C in 2022. On the other hand, the winters (December-January) are extremely chilly, recording a minimum temperature of -0.4°C . The entire

Gurgaon Administrative Division was considered here for the study, which was around 4171.89 km^2 .

2.2 Datasets used

MODIS (Moderate Resolution Imaging Spectroradiometer) images were collected from the National Aeronautics and Space Administration Level- 1 and Atmosphere Archive and Distribution System Distributed Active Archive Center (NASA LAADS DAAC). Data on clouds, water vapour and aerosols are distributed and archived by NASA LAADS DAAC. Table 1 represents all of the MODIS products downloaded for the specific dates for all three study regions in the summer (March) and winter (December) seasons with the least possible cloud cover. The dates are selected as such it

Table 1 Datasets used for the three study areas—Gandhinagar, Bongaigaon and Gurgaon

Study Area	Satellite & Instrument	Products Used	Spatial Resolution	Tile	Summer Dates	Winter Dates
Gandhinagar District	Terra MODIS	MOD11A1	1 km × 1 km	h24 v06	30 Mar 2006	30 Dec 2006
		MOD09A1	500 m × 500 m		13 Mar 2010	14 Dec 2010
		MCD12Q1	500 m × 500 m		13 Mar 2014	14 Dec 2014
Bongaigaon & Surroundings	Terra MODIS	MOD11A1	1 km × 1 km	h26 v06	26 Mar 2006	14 Dec 2006
		MOD09A1	500 m × 500 m		13 Mar 2010	14 Dec 2010
		MCD12Q1	500 m × 500 m		08 Mar 2014	28 Dec 2014
Gurgaon Administrative Division	Terra MODIS	MOD11A1	1 km × 1 km	h24 v06	19 Mar 2018	14 Dec 2018
		MOD09A1	500 m × 500 m		13 Mar 2022	14 Dec 2022
		MCD12Q1	500 m × 500 m		02 Mar 2006	19 Dec 2006
		MOD11A1	1 km × 1 km		13 Mar 2010	14 Dec 2010
		MOD09A1	500 m × 500 m		13 Mar 2014	16 Dec 2014
		MCD12Q1	500 m × 500 m		13 Mar 2018	14 Dec 2018
		MOD11A1	1 km × 1 km		13 Mar 2022	18 Dec 2022

falls in the mid-March and mid-December unless the period is affected by cloud cover.

With a spatial resolution of one kilometre (km), the MOD11 A1 Version 6 product provides daily per-pixel Land Surface Temperature (LST) and Emissivity (E) in a grid of $1,200 \times 1,200$ km. The value of the pixel temperature is obtained using the MOD11_L2 swath product. When the clear-sky requirements are met, certain pixels may have several observations above 30 degrees latitude. The pixel value in this case is determined by averaging all qualifying observations. Surface temperature bands for daylight and nighttime are accompanied by bands 31 and 32 emissivities from land cover categories, corresponding quality control assessments, observation times, view zenith angles, and clear-sky coverages (Wan et al. 2021).

With atmospheric factors including gases, aerosols, and Rayleigh scattering taken into account, the MODIS Terra MOD09 A1 Version 6 product offers an estimate of the surface spectral reflectance of Terra MODIS Bands 1 through 7. Four observation bands, two quality layers, and seven 500 m (m) reflectance bands are included. Out of all the acquisitions made throughout the eight-day composite period, a value is chosen for every pixel. Solar zenith and clouds are two of the pixel selection criteria. The pixel with the lowest channel 3 (blue) value is used when multiple acquisitions match the requirement (Vermote 2015).

Derived from six distinct classification schemes indicated in the User Guide, the Terra and Aqua combined Moderate Resolution Imaging Spectroradiometer (MODIS) Land Cover Type (MCD12Q1) Version 6 data product provides worldwide land cover types at yearly intervals (2001–2020). MODIS Terra and Aqua reflectance data supervised classifications are used to create the MCD12Q1 Version 6 data package. After that, the supervised classifications go through more post-processing to further hone in on particular classes by incorporating auxiliary

data and past knowledge (Friedl and Sulla-Menashe 2019). The product MCD12Q1 has performed well for Land Cover Classification over various studies. MCD12Q1 has shown good consistency and accuracy as per the Food and Agriculture Organisation (FAO) agreement when quantifying the relationship between cropland classification agreement and four other factors like slope, elevation, field size and crop agreement (Xue et al. 2024). For denoting the area of interest as per the study regions, Digital Vector Database in the form of shapefile were required, which were obtained from the Survey of India, Ministry of Science and Technology through their Online Maps Portal (<https://onlinemaps.surveyofindia.gov.in/>).

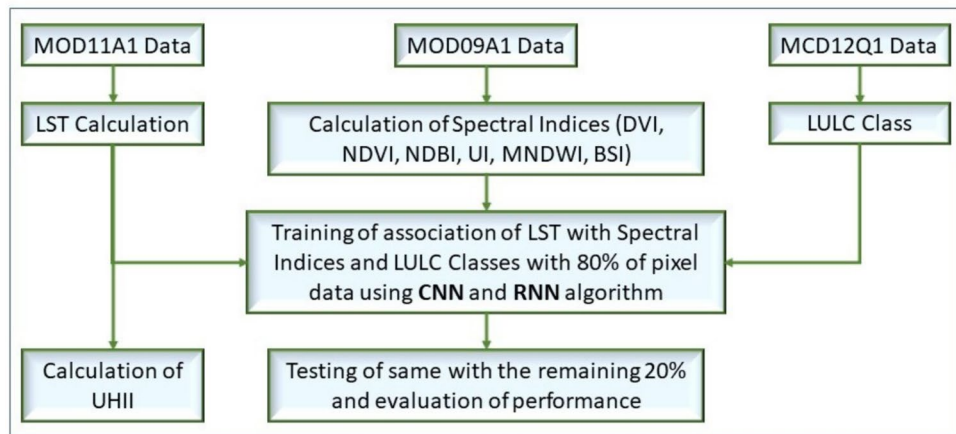
2.3 Data processing

The obtained MODIS products can be processed LST calculation, calculation of the various considered spectral indices and the respective LULC Classes. The association of LST with various spectral indices along with the LULC classes are modelled using two ML models – CNN and RNN with 80% of the pixel data used for training and the remaining is used for testing. The calculated LST is also used to calculate the UHII for the considered five cities amongst the three chosen study areas. The methods used are described comprehensively from Sect. 2.3 to Sect. 2.5. A flow chart summarizing pictorially the flow of the work is shown in Fig. 2.

2.3.1 Processing of land surface temperature (LST) data

NASA's Level- 1 and the Atmosphere Archive & Distribution System Distributed Active Archive Centre (LAADS DAAC, <https://ladsweb.modaps.eosdis.nasa.gov/>) provided the 8-day average, per-pixel MODIS/Terra LST data with a nominal spatial resolution of 1 km (MOD11 A1, version 6). The generalised split-window technique is used by the

Fig. 2 Flowchart of methodology



MOD11 A1 products to provide daily LST and emissivity values (Wan and Dozier 1996). They are employed to ascertain the MODIS observation period and whether clouds impacted the pixels corresponding to ground observation stations (sites). At grids where no valid pair of day and night observations exist, the generalised split-window algorithm was applied to supplement the LSTs retrieved by the day/night LST algorithm (Becker and Li 1990; Wan and Dozier 1996). The LST of the aforementioned study locations was determined in this investigation using MOD11 A1.

Typically, a MOD11 A1 product is delivered in Hierarchical Data Format (HDF), which includes LST information for the day and night of a given day. All MOD11 A1 data files have been downloaded as tiles that make up the area under examination. The projection system employed in this study was the World Geodetic System 1984 (WGS84). To get the LST in Kelvin, the pixel values are multiplied by the specific scale factor. A scale factor 0.02 was used for all the data files (Bala et al. 2020). After subtracting 273.15, the LST in degree Celsius will be obtained.

$$\text{LST}(\text{Day or Night}) \text{ in } ^\circ\text{C} = \text{Scale Factor} * \text{Pixel Value} - 273.15 \quad (1)$$

2.3.2 Calculation of the spectral indices

Surface reflectivity data can be obtained from Product MOD09 A1, which can also be downloaded from the same source as MOD11 A1. The spatial resolution of MOD09 A1 is 500 m with 7 bands, and the centre of each band is 646 nm, 858 nm, 470 nm, 555 nm, 1240 nm, 1640 nm, and 2130 nm, respectively (Vermote 2015). The spectral indices for each pixel can then be calculated following the radiation calibration and geometric correction processes. For this investigation, the following wavelengths are employed: Red, Green, Blue, Near Infrared (NIR), Shortwave Infrared

1 (SWIR1), and Shortwave Infrared 2 (SWIR2). These have been used to calculate the following spectral indices.

Difference vegetation index (DVI) The Difference plant Index (DVI) allows for the distinction between soil and plant. However, it does not consider atmospheric factors or shadows when calculating reflectance and radiance differences. It is essentially the distinction between the red and near-infrared spectrums (Gallo and Flesch 1989).

$$\text{DVI} = \text{NIR} - \text{Red} \quad (2)$$

Normalized difference vegetation index (NDVI) The Normalised Difference Vegetation Index, or NDVI, is a tool for measuring green vegetation and analysing plant health changes and density. Conventionally, the near-infrared (NIR) and red (R) measurements are compared to compute the NDVI (Petrolli 2013).

$$\text{NDVI} = \frac{\text{NIR} - \text{Red}}{\text{NIR} + \text{Red}} \quad (3)$$

Normalized difference built-up index (NDBI) The Normalised Difference Built-up Index (NDBI) highlights artificially created built-up regions with the use of the NIR and SWIR bands. It is ratio-based to reduce the impact of atmospheric effects and variations in terrain illumination (Zha et al. 2003).

$$\text{NDBI} = \frac{\text{SWIR1} - \text{Red}}{\text{SWIR1} + \text{Red}} \quad (4)$$

Urban index (UI) The concept of Urban Index (UI) was initially presented by (Kawamura 1996). It was based on a computer system that used the brightness relationship between urban regions and the near-infrared (0.76 to 0.90 μm) and mid-infrared (2.08 to 2.35 μm) spectrums. It utilises the NIR channel and Short-Wave Infrared (SWIR2) (Kawamura 1996).

$$UI = \frac{SWIR2 - Red}{SWIR2 + Red} \quad (5)$$

Modified normalised difference water index (MNDWI) The Modified Normalised Difference Water Index, or MNDWI, can be used to track changes in the water content of water bodies or leaves, depending on the type of remote sensing data used. It was chosen over Normalised Difference Water Index (NDWI) as the later is not sufficient for extracting shallower part of water bodies and is often erroneous in differentiating water body and built-up areas (Xu 2005).

$$MNDWI = \frac{Green - NIR}{Green + NIR} \quad (6)$$

Bare soil index (BSI) The Bare Soil Index (BSI) is a numerical indicator that incorporates blue, red, near-infrared, and short-wave infrared spectral bands to represent soil changes. The normalised difference is calculated (Diek et al. 2017) as follows:

$$BSI = \frac{(SWIR2 + Red) - (NIR + Blue)}{(SWIR2 + Red) + (NIR + Blue)} \quad (7)$$

2.3.3 Land use land cover (LULC) processing

Land cover data is produced by the MODIS Land Cover Dataset package MCD12Q1. The MODIS MCD12Q1 product was made available by NASA, and it identified several types of land cover using “annual observations” from the “Terra and Aqua satellites”. A Sinusoidal grid with approximately 10×10 slices is used to exhibit MCD12Q1 data in a hierarchical (HDF) format. For raw data, image pre-processing is first necessary and usually entails image enhancement, terrain correction, and geometry correction. The data is projected using the UTM WSG-84 in order to ensure consistency (Liang et al. 2015).

Land cover classification The MCD12Q1 product of MODIS provides Land Cover Type 1: Annual International Geosphere-Biosphere Programme (IGBP) classification at yearly intervals in Hierarchical Data Format 4 (HDF4) format which is convertible to raster images. The data obtained from the raster images are extracted through image classification and the resultant images are utilized in LULC maps. Reclassified options in ArcGIS were utilised to recode the grid code according to classification (Chowdhury 2023). “Water bodies, vegetation, built-up, agricultural & fallow, and barren land” were the five main categories into which the research regions were classified. Corresponding confusion matrix for validation of the LULC of the three study regions along with the calculated kappa coefficients validated with satellite imagery of Google Earth is provided in the appendix.

2.4 Calculation of urban heat island intensity (UHII)

UHI may be assessed in two ways:

- i) by delineating a particular urban–rural boundary and evaluating the LST difference between those two regions (Xu et al. 2024), or
- ii) by defining a certain threshold temperature difference to denote UHI effect and identifying the high and low temperature areas (Xu et al. 2024; Chen et al. 2021).

In the present study, the former assessment of UHI is adopted. Urban Heat Island Intensity (UHII) is the difference of the averaged LST of the urban area and the averaged LST of the surrounding non-urban area (Zou et al. 2021). As stated earlier, the LST data is obtained from the pixels of the MOD11 A1 product for a particular study area. The average of the pixel values falling within the urban area will give the Mean Urban LST (T_u) and the average of the pixel values encompassed by the non-urban area shall give the Mean Non-Urban LST (T_{nu}). In general, the Mean Urban LST is greater than the Mean Non-Urban LST which signifies the UHI. However, sometimes, the Mean Urban LST may be lesser than the Mean Non-Urban LST which signifies the development of an Urban Cool Island (UCI). Hence, UHII or UCII is given by

$$UHII \text{ or } UCII = T_u - T_{nu} \quad (8)$$

In this study, the primary focus was to investigate the UHI/UCI effect in the study regions. If UHII value is found to be negative, then that it is considered as UCI. When UHII values are found to be positive, then their magnitudes are compared. A city with higher positive UHII value is said to have a stronger Urban Heat Island Intensity.

2.5 Modeling the association of LST with spectral indices and LULC classes through ML algorithms

The association of different spectral indices and LULC classes with LST was investigated using the potential of machine learning approaches. Eighty percent (the first four years) of the data was used to train the model and the remaining twenty percent (the final year) to assess the model's accuracy. The different datasets have different spatial resolutions and the LST data is obtained at the coarsest resolution amongst all the other raster products i.e., 1 km. Hence, for maintaining uniformity, every raster variable utilized in the study, including LST, DVI, NDVI, NDBI, UI, MNDWI, BSI, and LULC class are regridded to a common resolution of 0.01 degrees (~ 1.11 km) (Cersosimo et al. 2020).

2.5.1 Modeling LST using the information of spectral indices and LULC classes

The association of LST with spectral indices—DVI, NDVI, NDBI, UI, MNDWI, BSI and LULC classes are modelled using the potential of two network-based Machine Learning approaches—Convolutional Neural Network (CNN) and Recurrent Neural Network (RNN). The ML algorithms were implemented in Python using the packages ‘keras’ and ‘tensorflow’.

Convolutional neural network (CNN) CNNs largely focus on the idea that the input will be comprised of images. This concentrates on how the architecture should be configured to best meet the requirements for handling the particular kind of data. Neural layers of a CNN are composed of three-dimensional neurons arranged according to the input's spatial dimensions (height, breadth, and depth) (Venkatesan and Li 2017). The pixel values of the image will be stored in the input layer. By calculating the scalar, the convolutional layer will ascertain the output of neurons that are related to certain parts of the input (O'Shea and Nash 2015). Subsequently, a pooling layer will downsample the input along its spatial dimensions, which will further reduce the number of parameters in that activation (Gholamalinezhad and Khosravi 2020). Finally, the output from the fully-connected layers will be determined by the calculations made in the earlier levels using, the required activation function (O'Shea and Nash 2015). To improve model accuracies, the required parameters such as the optimizer, learning rate, epochs, batch size, and neuron layer architecture can be altered accordingly (Pasi and Naik 2016). Zheng et al. (2016) have shown the accuracy of effective transfer of CNN models in image search and classification. Deep CNN has bettered other known methods in ImageNet Large-Scale Visual Recognition Challenge (ILSVRC) 2012 (Russakovsky et al. 2015). This study uses processed raster images from the MODIS products mentioned in Sect. 2.2. Raster images can be well studied and analysed using computer vision and Deep CNN techniques for their ability to contain and visualise a huge number of layers (Dao and Zettsu 2018). CNN has performed for tackling image-based issues because it utilises information from adjacent pixels of a raster with significantly less trainable parameters than other ML methods (Ouma and Omari 2023). Further details about CNNs may be obtained from several studies (O'Shea and Nash 2015; Gu et al. 2018).

Recurrent neural network (RNN) An improved RNN type for managing long-range dependencies is called a Long Short-Term memory (LSTM) (Sundermeyer et al. 2012) which is employed in the present study. LSTMs have gates (forget gate, output gate, and input gate) to regulate data flow and prevent problems like exploding and vanishing gradients (Gers et al. 1999; Arpit et al. 2018). The memory cell, which can store information for extended periods of time, is the main component of an LSTM (Pulver and Lyu 2017).

The input gate determines the amount of new input that should be added to the memory cell whereas forget gate determines the part of the past memories to forget. The output gate takes care of how much of the memory cell should be used to compute the output (Staudemeyer and Morris 2019). For improved model accuracies, variables like as the learning rate, optimizer, epochs, and neuron layer structure can be changed (de Moura et al. 2022). LSTM combined with conv1D has a good accuracy for image recognition (Phiphatphaisit and Surinta 2021). Several MODIS products (mentioned in Sect. 2.2) were used as raster for the study. A combination of CNN-LSTM has performed better when compared to ConvLSTM when working with raster of remote sensing images (Bounoua et al. 2024). An NDVI time series prediction model generated from multi-layer multivariate LSTM studied on rasters of MOD13 A2 of MODIS can predict future changes in the surface vegetation with greater accuracy (Guo et al. 2024). Further details about LSTMs may be obtained from several studies (Sundermeyer et al. 2012; Staudemeyer and Morris 2019).

3 Results

3.1 LULC changes over the study period

From the MODIS product MCD12Q1, the LULC Maps were produced for all the three study regions. Gandhinagar and Bongaigaon primarily had five classes—Vegetation, Water Body, Built-up Area, Agricultural & Fallow and Barren, whereas Gurgaon had three classes only comprising Vegetation, Built-up Area and Agricultural & Fallow.

From 2006 to 2022, the LULC change for each of the aforementioned classes in Gandhinagar has been monitored for five distinct years at a time-step of four years which is shown in Fig. 3 and summarized in Table 2. There is a scarcity of a noticeable water body throughout the years. In 2022, the amount of natural vegetation in the study region, decreased to 0.06% from approximately 3.55% in 2006. Moreover, the percentage of barren land decreased from 0.28% in 2006 to 0.08% in 2022. The built-up area has not changed significantly. The percentage of land used for agriculture and fallows rose from 91.57% in 2006 to 95.15% in 2022. It is possible to conclude that, in comparison to 2006, the majority of the areas that were once vegetated and barren have now been converted to agricultural and fallow lands.

The LULC changes in Bongaigaon are presented in Fig. 4 and summarized in Table 2. Both the percentage of built-up area and water bodies decreased slightly during the study period. Water bodies declined from 7.39% in 2006 to 6.37% in 2022, though the changes were extremely small. In contrast, the built-up area first decreased from 14.65% in 2006 to 12.99% in 2014 before increasing to 13.25% in 2022. This can be

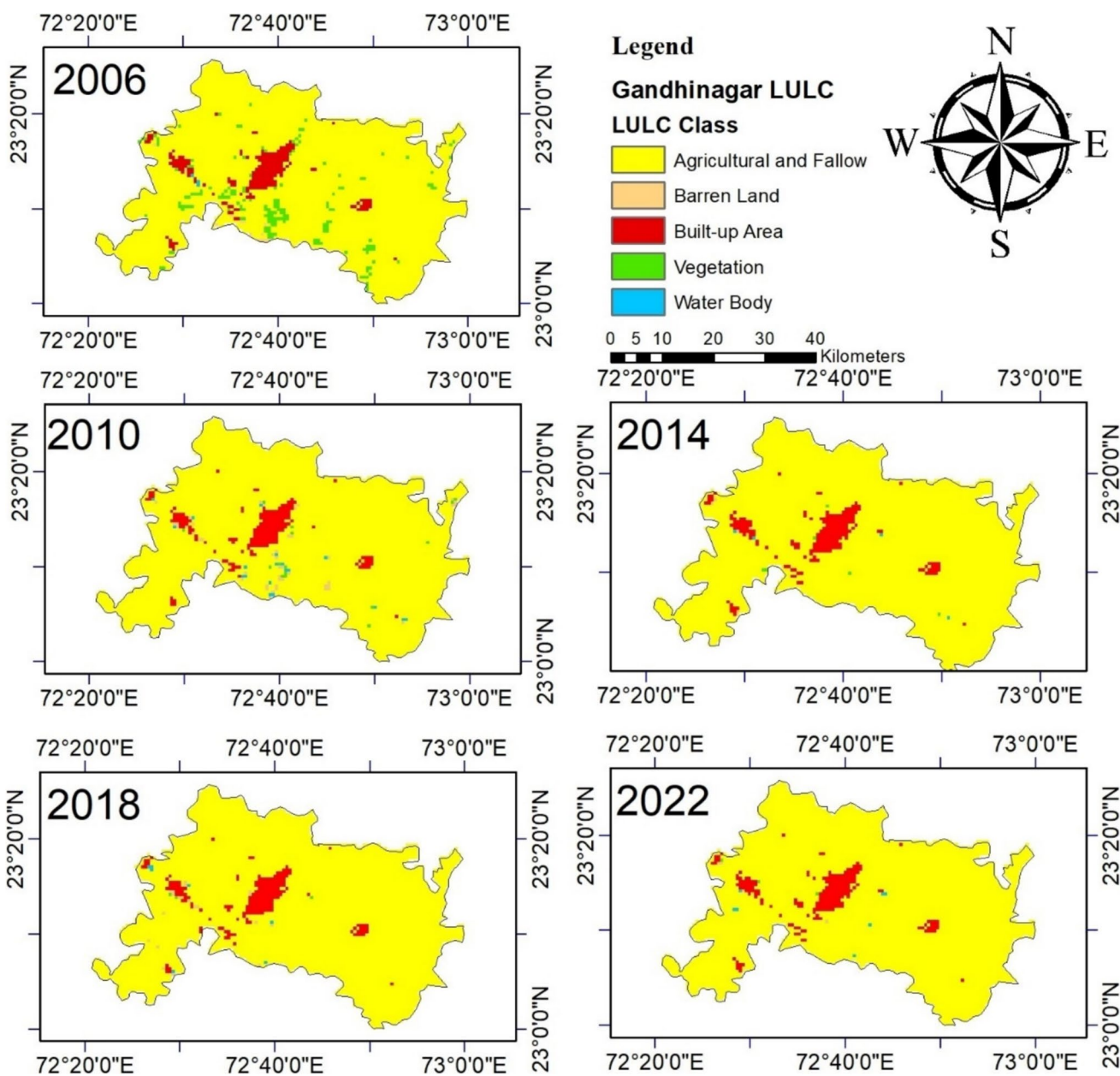


Fig. 3 Gandhinagar LULC changes for 2006 to 2022

accounted to the urbanization being done at the cost of filling up of water bodies. Although the amount of land used for agriculture and fallow crops has not changed over time, the percentage of the barren land has dropped from 7.52% in 2006 to 3.95% in 2022. The fact that the percentage of vegetation increased from 18.98% in 2006 to roughly 24.2% in 2022 portrays that nearly one-fourth of the study region consists of natural greenery in the year 2022. This increment in vegetation was also witnessed within the urban area of the considered study region.

The LULC changes in Gurgaon are presented in Fig. 5 and summarized in Table 2. Gurgaon had typically three types of classes—Vegetation, Built-up area and Agricultural and

fallow land. Large water bodies or significant unused barren land were two unprocurable classes from the LULC maps of Gurgaon, as the considered study area did not have any reasonable area enough to be classified into these two classes. Among the available classes, the agricultural and fallow land significantly declined from 85.53% to 77.85% over the span of these 16 years. Like the other developing cities, the city of Gurgaon expanded over time, which is evident from the increase in built-up area from 9.86% in 2006 (of the considered study area) to 13.17% in 2022. Conversion of barren lands into agricultural or vegetation or conversion of agricultural land to vegetation can help in restricting rise of LST (Pandey et al. 2023a). Despite the

Table 2 Area of LULC classes for different study area with percentages from year 2006 to 2022

Study Area	LULC Class	2006		2010		2014		2018		2022	
		Area (sq. km)	%								
Gandhinagar	Water Body	3.70	0.06	23.41	0.39	4.93	0.08	8.62	0.14	8.62	0.14
	Vegetation	215.62	3.55	18.48	0.30	7.39	0.12	3.70	0.06	3.70	0.06
	Built-up Area	275.99	4.54	257.51	4.24	277.22	4.56	262.44	4.32	277.22	4.56
	Agricultural and Fallow	5564.16	91.57	5723.10	94.18	5781.01	95.13	5778.55	95.09	5782.25	95.15
	Barren Land	17.25	0.28	54.21	0.89	6.16	0.10	23.41	0.39	4.93	0.08
	Total	6076.72	100.00	6076.72	100.00	6076.72	100.00	6076.72	100.00	6076.72	100.00
Bongaigaon	Water Body	71.46	7.39	75.16	7.77	72.69	7.52	54.21	5.61	61.61	6.37
	Vegetation	183.58	18.98	267.37	27.64	255.04	26.37	225.47	23.31	234.10	24.20
	Built-up Area	141.69	14.65	135.53	14.01	125.67	12.99	130.60	13.50	128.14	13.25
	Agricultural and Fallow	497.77	51.46	415.22	42.93	441.09	45.61	508.86	52.61	505.16	52.23
	Barren Land	72.69	7.52	73.93	7.64	72.69	7.52	48.05	4.97	38.20	3.95
	Total	967.20	100.00	967.20	100.00	967.20	100.00	967.20	100.00	967.20	100.00
Gurgaon	Vegetation	192.21	4.61	129.37	3.10	284.62	6.82	220.55	5.29	374.56	8.98
	Built-up Area	411.52	9.86	462.04	11.08	517.48	12.40	527.34	12.64	549.52	13.17
	Agricultural and Fallow	3568.16	85.53	3580.48	85.82	3369.79	80.77	3424.01	82.07	3247.82	77.85
	Total	4171.89	100.00	4171.89	100.00	4171.89	100.00	4171.89	100.00	4171.89	100.00

expanding city, the vegetation percentage increased from 4.61% in 2006 to 8.98% in 2022. But this increment was observed because of the vegetative developments around the vicinity of the city as the slight patches of vegetation within the city had actually reduced over the years.

A detailed confusion matrix for all the three study regions along with overall accuracy and kappa coefficient of the LULC maps thus obtained from MCD12Q1 when compared with Google Earth Satellite Imagery is provided in Tables 3, 4 and 5.

3.2 Spatial and temporal variation of LST

The spatial and temporal variation of LST were presented in the form of maps after processing the MOD11 A1 product of MODIS. The LST maps of the three study regions during the study period is shown in Fig. 6 (Gandhinagar), Fig. 7 (Bongaigaon) and Fig. 8 (Gurgaon). White spaces (if any) on the maps represent the missing values. It is interesting to note that, in addition to the main city of Gandhinagar, there were two other small cities close to Gandhinagar where local LST was higher than the surrounding region. One is Dahegam on to the east of Gandhinagar and another was Kalol, to the west of Gandhinagar. This indicates the presence of UHI effect. Thus, the UHII was also investigated for these two smaller cities. Averaged LST values of each LULC category for all the three study areas are provided in Table 6.

3.3 Urban heat island intensities

UHII was calculated for five cities—Gandhinagar, Dahegam, Kalol, Bongaigaon and Gurgaon. As explained in Sect. 2.4, UHII is given by the difference between the average LST of the pixels within the city and the average LST of the pixels surrounding the city. A table of urban Temperature (T_u), non-urban Temperature (T_{nu}) and UHII values for all the five cities for five years from 2006 to 2022 for both summer and winter is presented in Tables 7, 8, 9, 10 and 11 in the appendix.

Gandhinagar mostly had a mild UHII during the daytime in the summers with an UHII value of less than 1 °C. But during the night, it triggered to intensities greater than 1 °C. During the winters, the daytime UHII were very less and sometimes negative, indicating Urban Cool Island (UCI) (Martins et al. 2016) and again in nocturnal period it was mostly above 1 °C similar to that in summers. Dahegam mostly had a highly intensified UHII even up to 2.27 °C during the daytime in summers. Though it's a considerably smaller urban region than the state capital Gandhinagar, but the UHI effect in daytime during summers was way higher. Nights were cooler in the city during the summers with UHII mostly less than 1 °C probably due to lesser building heights. Rezaei et al. (2020) have already showed that the planning of taller buildings will lead to the augmentation of LST and hence lesser building heights have saved Dahegam from the grasp of nighttime UHI. The daytime of the winters has witnessed negative UHII values, indicating an UCI effect. However, the nights of winter experience a mild

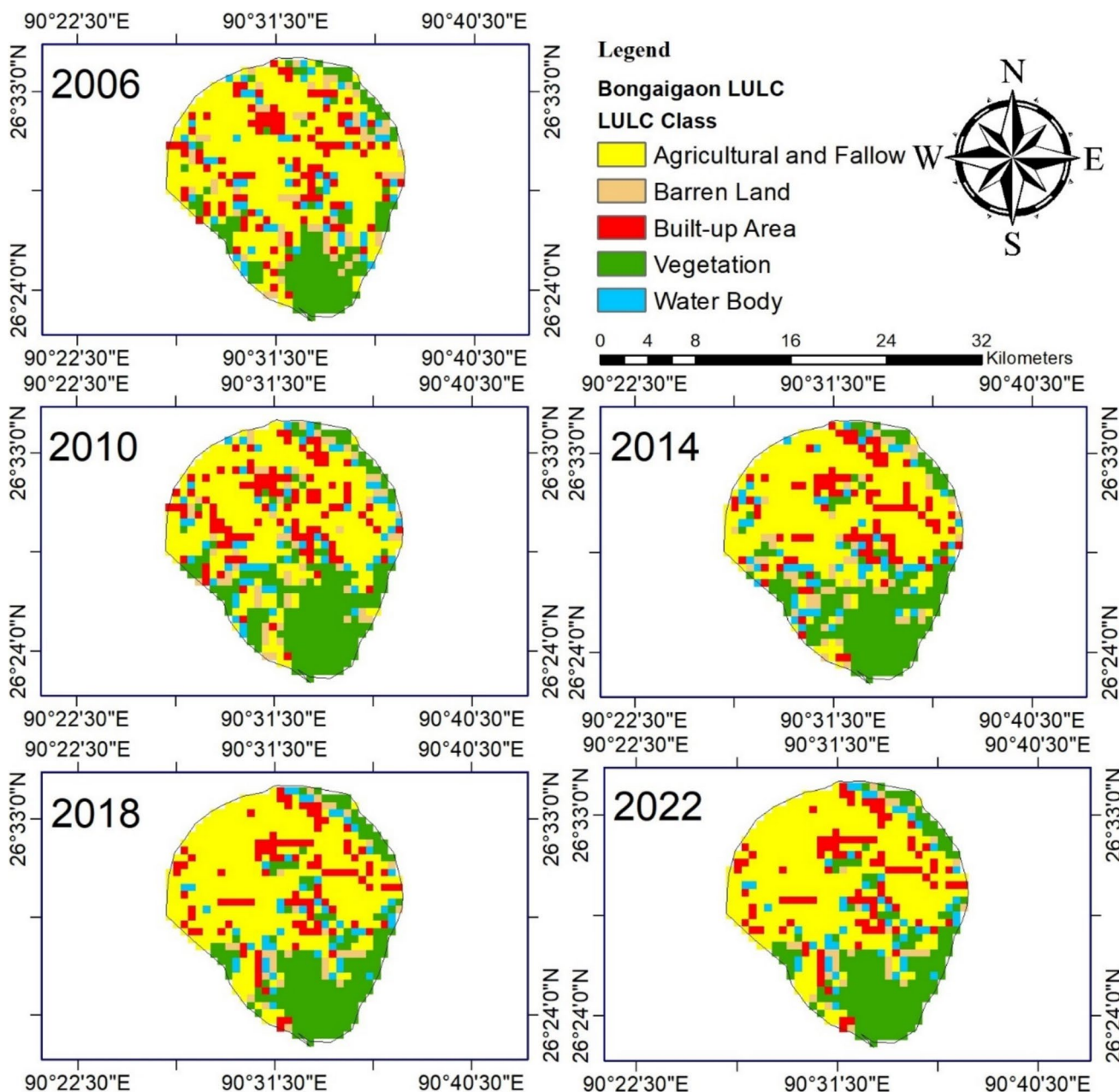


Fig. 4 Bongaigaon LULC changes for 2006 to 2022

UHII less than 1 °C. Kalol had daytime UHII at summers less than 1 °C. Night time mostly had UHII greater than 1 °C.

Bongaigaon, due to its large amount of vegetation even within the city has UCI in daytime for winters and even in summers. Even though there are formations of UHI at night in Bongaigaon, during both summers and winters but the intensities were mostly less than 1 °C.

The UHII's were highest in Gurgaon due to its highly built-up land cover. The daytime in summers mostly had UHII more than 1 °C, whereas nighttime UHII's were as high as above

3 °C during summers. Gurgaon shows UCI during the daytime of winters; however, during the nighttime UHI intensifies to above 2 °C.

The UHII/UCII values for all the five cities for 2006, 2010, 2014, 2018 and 2022 were plotted and represented in the form of bar graphs as shown in Fig. 8. The intensity is mostly positive, i.e., UHI is being experienced mostly for all the five cities during summer days (Fig. 9a) and summer nights (Fig. 9b). For winter days (Fig. 9c) the cities many a time have experienced a UCI effect but again they

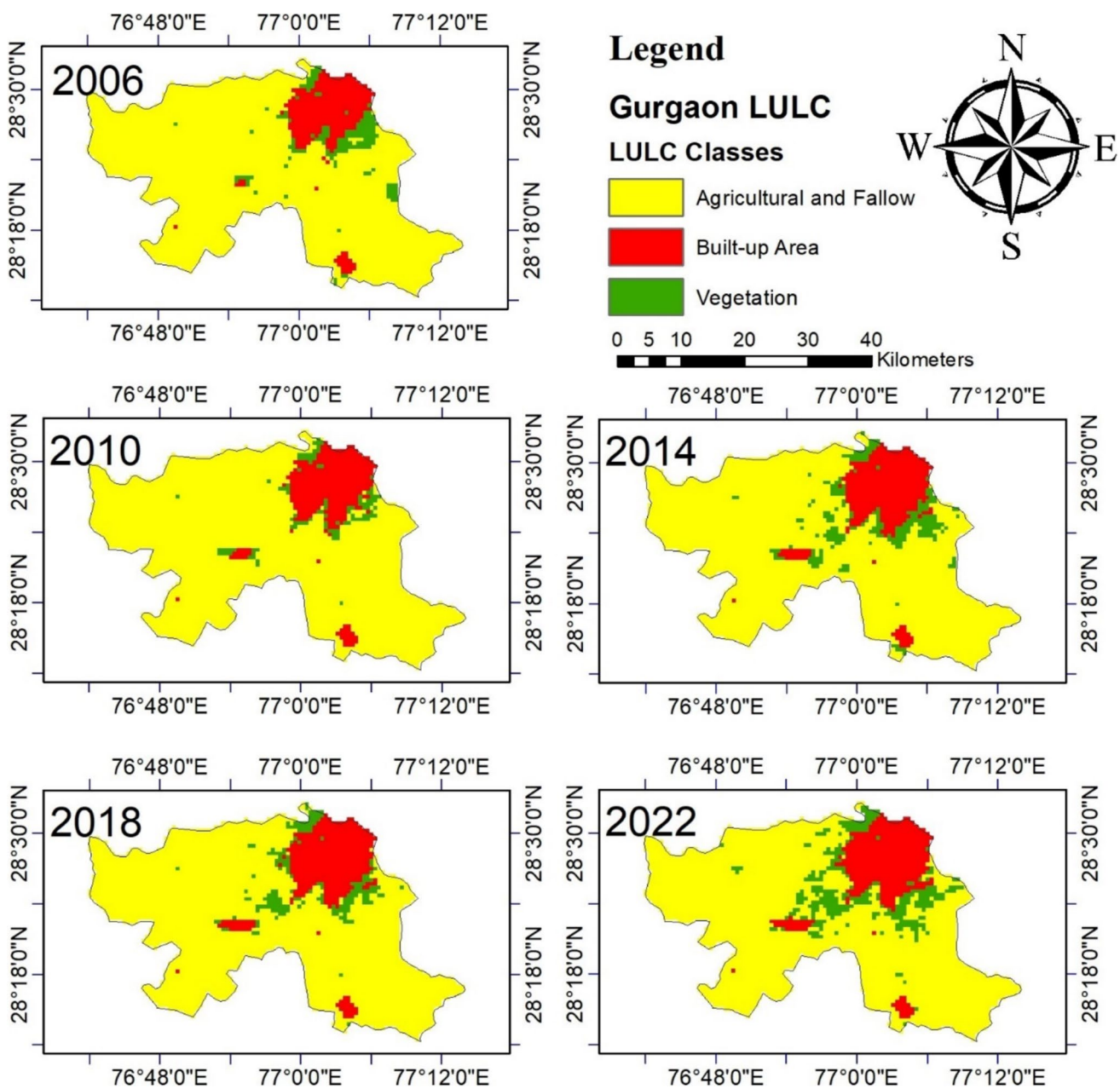


Fig. 5 Gurgaon LULC changes for 2006 to 2022

experience mostly a UHI of considerable intensity during winter nights (Fig. 9d).

3.4 Modeling LST of Gandhinagar, Bongaigaon and Gurgaon using the information of spectral indices and LULC classes

As mentioned in Sect. 2.5, the potential of ML models is utilized to estimate the LST of Gandhinagar, Bongaigaon and Gurgaon using the corresponding information of spectral

indices and LULC classes along with suitable interpolation for the missing values.

3.4.1 Results from CNN regression

One-Dimensional CNN model was developed with two hidden layers each with Rectified Linear Unit (ReLU) activation function. The learning rate was varied between 0.001 to 0.01 to obtain the best results. Regression analysis was performed using the CNN method on both training and testing period of

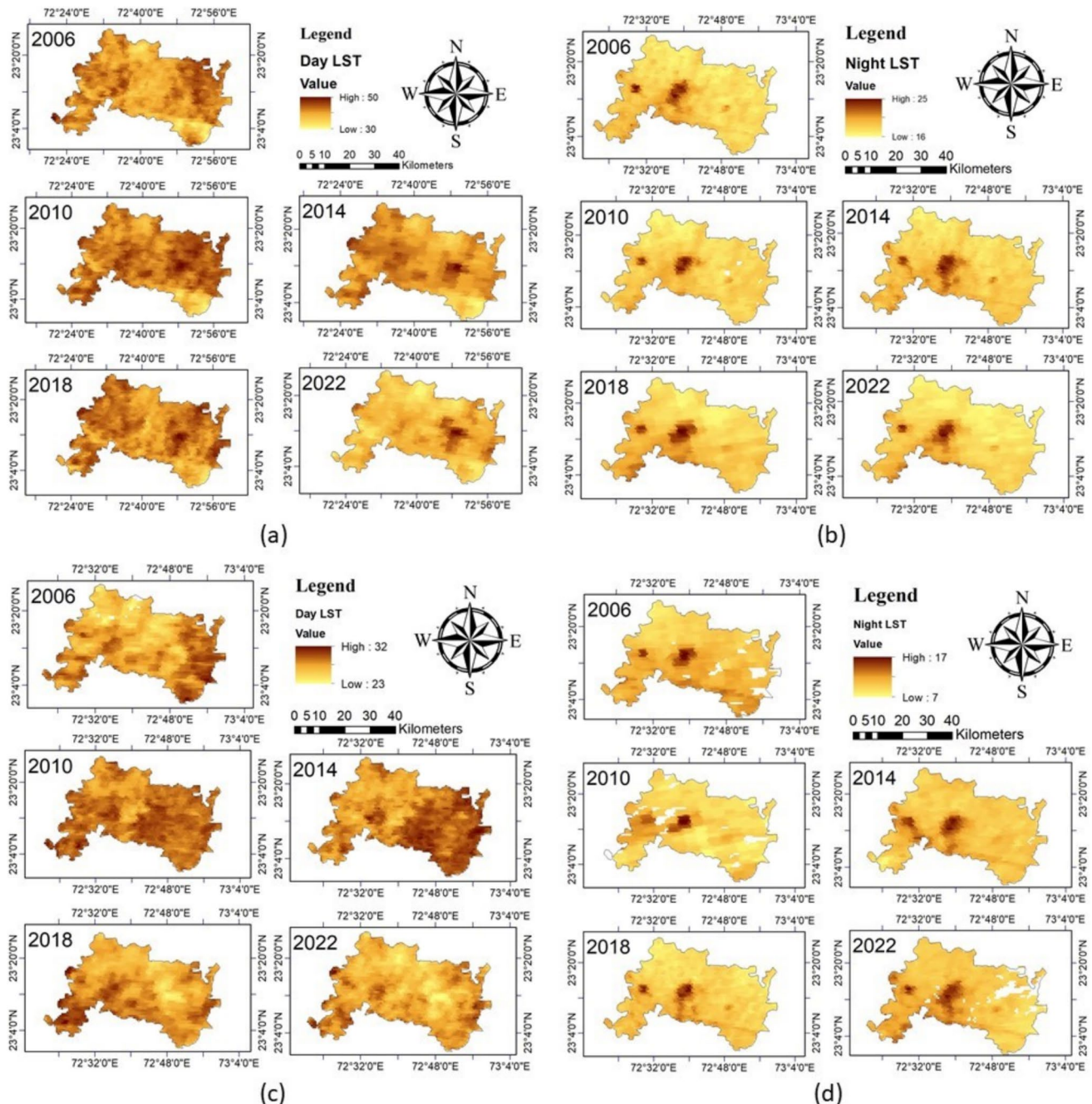


Fig. 6 LST map of Gandhinagar district for years 2006, 2010, 2014, 2018 and 2022 for (a) summer day, (b) summer night, (c) winter day and (d) winter night

Gandhinagar, Bongaigaon and Gurgaon study areas to compare the observed and modelled values. The scatter plots of the training period are presented in the Appendix in Fig. 11 and those of the testing period are presented in Fig. 10. For Gandhinagar, it was noted that the coefficient of determination (R^2) values for the daytime training and testing period, and nighttime training and testing period during the summer were, respectively, 0.863, 0.828, 0.881, and 0.776 (Figs. 11a and 10a). The r-squared

values were marginally better for the winter. It was revealed that the r-squared figures for the daytime training and testing, and nighttime training and testing period for winter were 0.829, 0.850, 0.940 and 0.851 respectively.

For Bongaigaon, during summers, the r-squared values were found to be 0.982, 0.738, 0.981 and 0.938 for daytime training and testing and nighttime training and testing respectively. During winters, the corresponding values were 0.991,

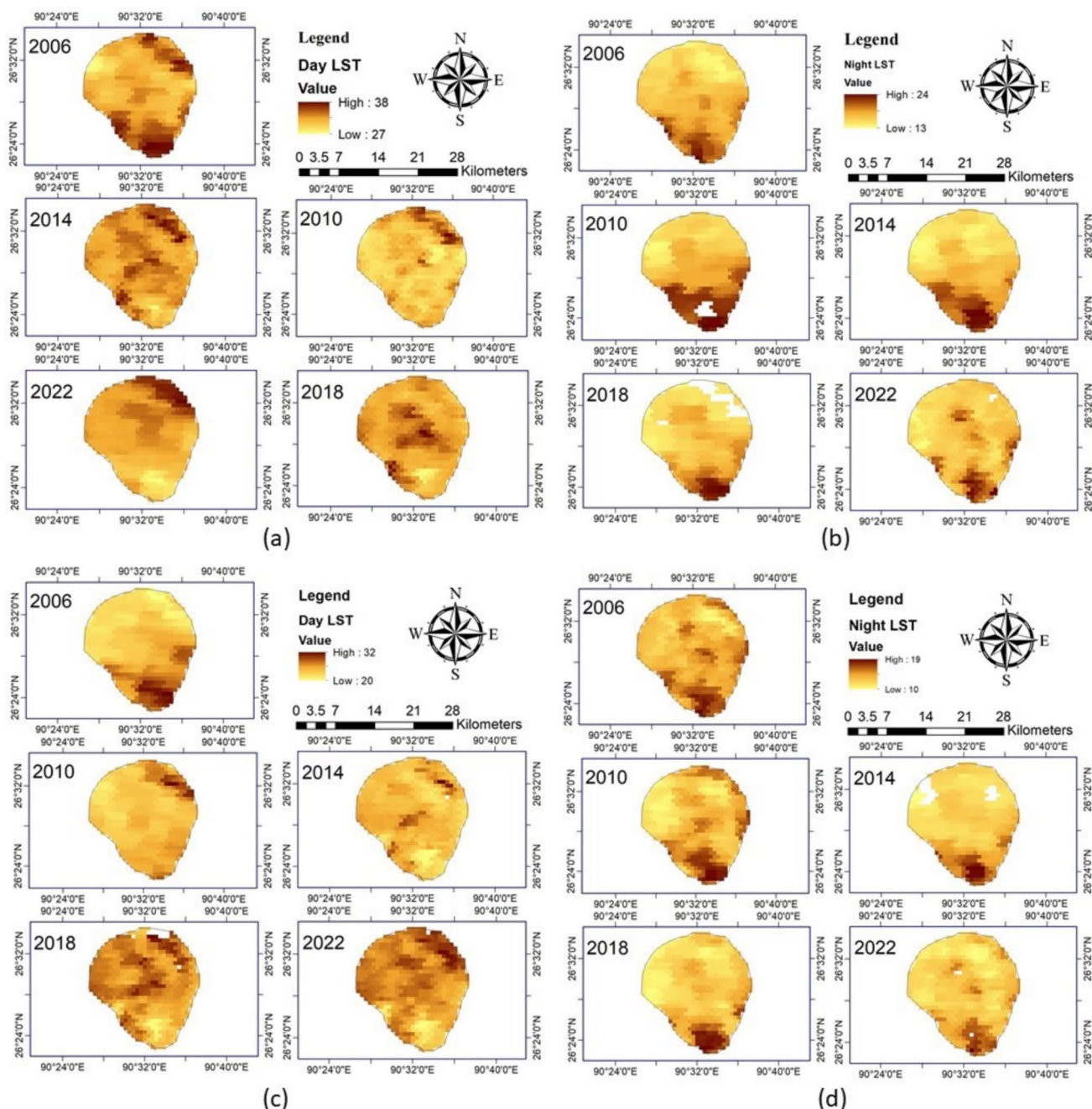


Fig. 7 LST Map of Bongaigaon city and its surroundings for years 2006, 2010, 2014, 2018 and 2022 for (a) summer day, (b) summer night, (c) winter day and (d) winter night

0.936, 0.987 and 0.944 respectively for daytime training and testing and nighttime training and testing. A movement in the plot toward higher LST, primarily for the testing plots conducted for later years, suggests that, in contrast to Gandhinagar, Bongaigaon has warmed with time (Figs. 11c and 10c).

For Gurgaon area, the r-squared values for daytime training and testing and nighttime training and testing throughout the summers were determined to be 0.988, 0.911, 0.916, and 0.940, respectively. In the winter, the results for training

and testing during the day and at night were, respectively, 0.982, 0.906, 0.898, and 0.891. A shift in the test plots values towards higher values when compared to the train suggests that Gurgaon's LST has increased over time (Figs. 11e and 10e).

The comparatively lower values of the r-square sometimes during the summers as compared to that the winters can be accounted to the lesser association of spectral indices with LST during summers which possibly could

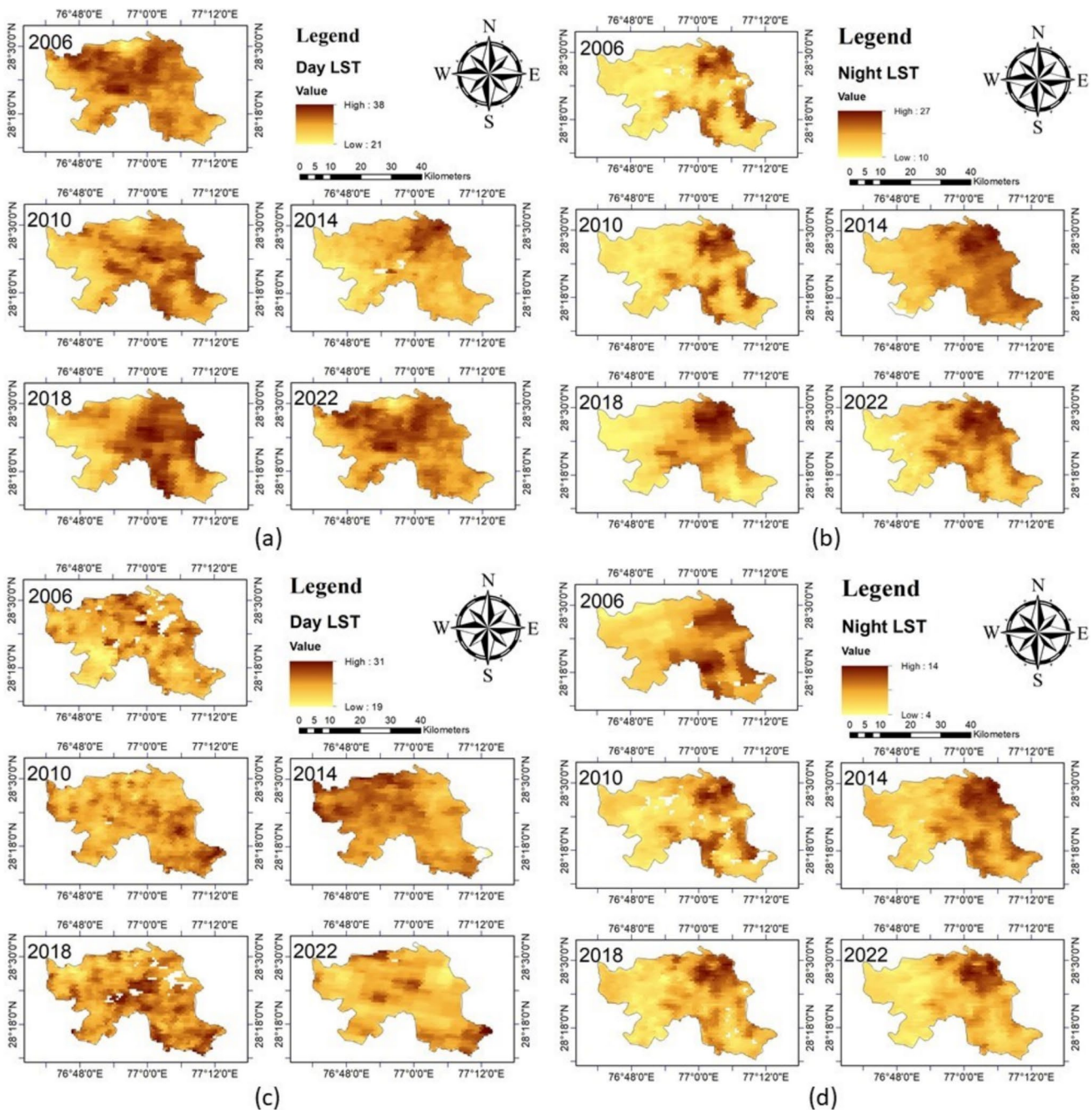


Fig. 8 LST Map of Gurgaon administrative division for years 2006, 2010, 2014, 2018 and 2022 for (a) summer day, (b) summer night, (c) winter day and (d) winter night

be due to the high variability of moisture content (Pandey et al. 2022) thus letting the model perform better in the winters.

3.4.2 Results from RNN regression

An LSTM Model was developed to predict the LST of the three study regions. The model had two hidden layers activated by ReLU function and learning rate varied between

0.001 to 0.01 to obtain best possible results. Gandhinagar's training and testing periods were subjected to regression analysis utilizing the RNN approach in order to compare the observed and modelled values. When compared to CNN's regression analysis, the results were substantially better. As seen in Figs. 11b and 10b, it was found that the r-squared values for the Gandhinagar training and testing data recorded during the day and at night throughout the summer were, respectively, 0.995, 0.967, 0.983, and 0.980. For the winter,

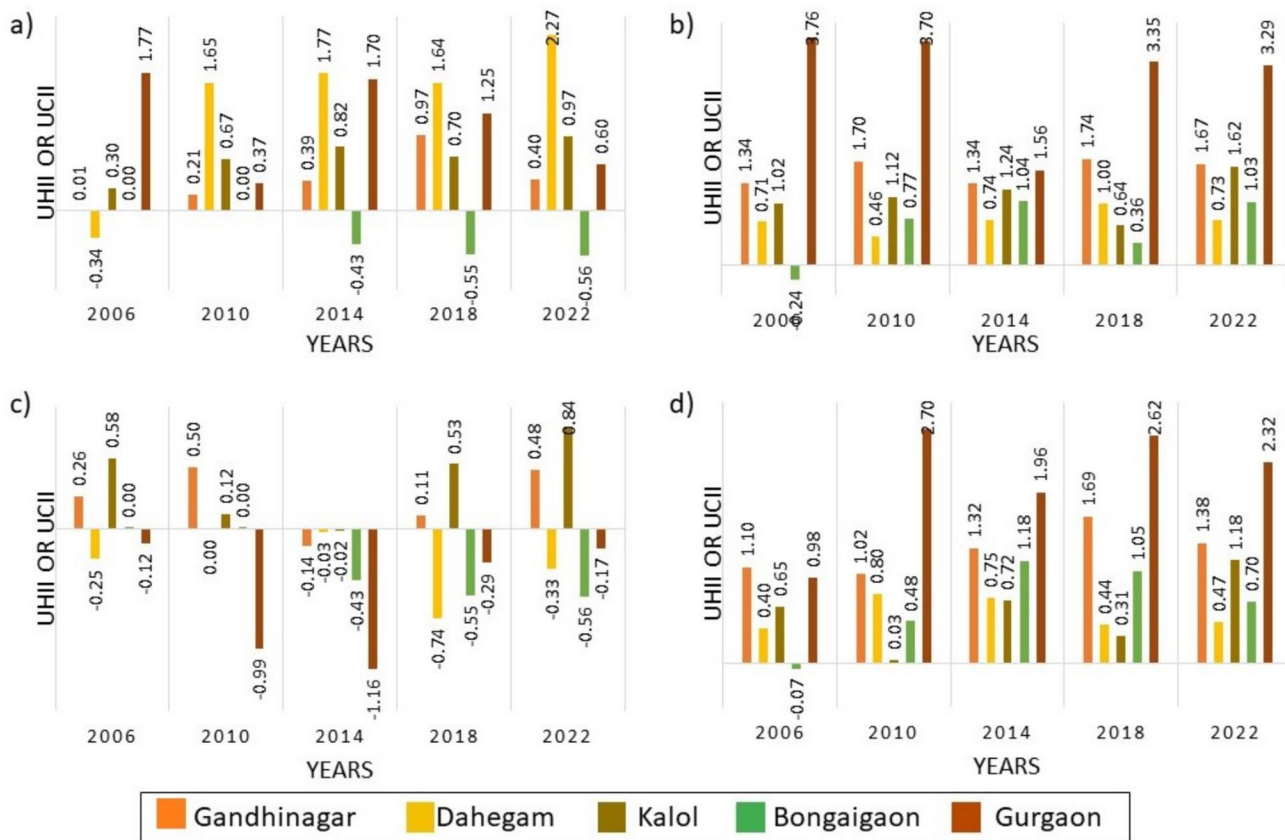


Fig. 9 UHII plots for all the cities from for years 2006, 2010, 2014, 2018 and 2022 for (a) summer days, (b) summer nights, (c) winter days and (d) winter nights

the r-squared values for the training and testing data during the day and the training and testing data during the night for the winter were found to be, respectively, 0.987, 0.979, 0.997, and 0.967 (Figs. 11b and 10b).

For Bongaigaon Study Area, the r-squared values for the modelled LST values for the training and testing period during the day and at night throughout the summer were determined to be, respectively, 0.994, 0.900, 0.995, and 0.961, as shown in Figs. 11d and 10d. The corresponding values for winter were 0.995, 0.969, 0.996, and 0.915, respectively (Figs. 11d and 10d). The LST values are larger in magnitude during the test period indicating a rise in LST in later years.

In Gurgaon also, the LST estimates with RNN showed improvement. The r-squared values for the Gurgaon Study Area's training and testing period during the day and at night throughout the summer were determined, respectively, 0.993, 0.904, 0.977, and 0.978, as shown in Figs. 11f and 10f. For winter, the corresponding values were 0.940, 0.811, 0.982, and 0.970, respectively (Figs. 11f and 10f). Similar to Bongaigaon, higher LST values during test period reaffirm rise in LST in recent years in Gurgaon. A table (Table 12) is also provided to summarise the obtained R² values of both CNN and RNN model for the three study

regions for both day and night of summer and winter respectively.

4 Discussions

It is evident from the confusion matrix (Tables 3, 4 and 5) that the LULC maps obtained from the MCD12Q1 product of MODIS are quite accurate. There is a decline of vegetation in Gandhinagar from 2006 to 2010 and a large declination of shrubs has also been confirmed by Purswani et al. (2022). Urban sprawl and settlements pointing toward the nearby city of Ahmedabad were also evident in the study, in agreement with some previous studies (Purswani et al. 2022). Sabarmati River is mostly dry until southern Gandhinagar; the river fills up largely thereafter. The sudden upsurge in the percentage in water bodies during 2006–2010 is due to the construction of the Narmada Water Canal which is built across the river between Ahmedabad and Gandhinagar during the period before its inauguration on April 24, 2008 (Debsarma et al. 2023). Constant deforestation and conversion of vegetative land to bare land and again using up of barren land for agricultural purposes lead to fluctuation of the barren land percentage simultaneously

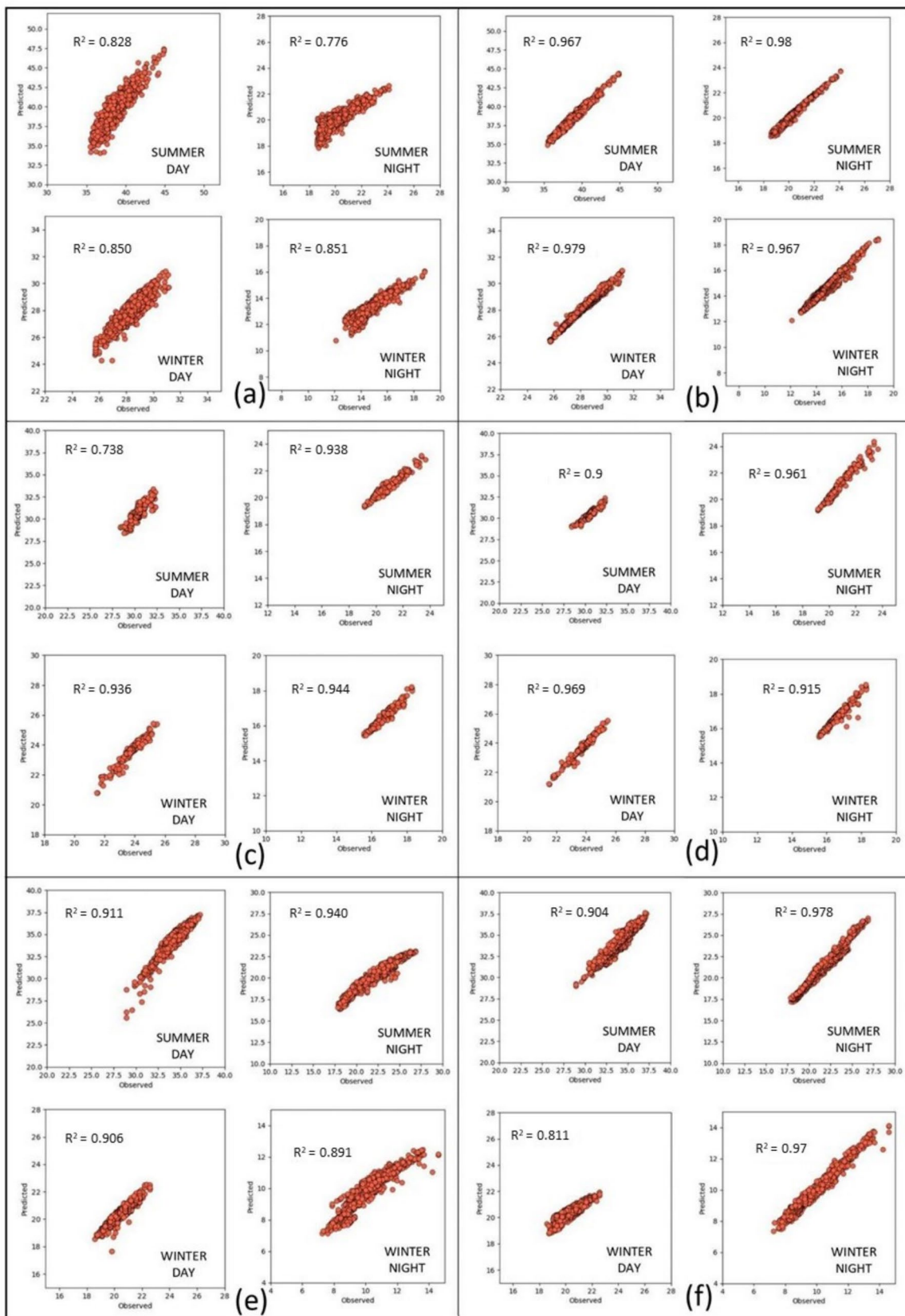


Fig. 10 Test plots of (a) CNN for Gandhinagar, (b) RNN for Gandhinagar, (c) CNN for Bongaigaon (d) RNN for Bongaigaon, (e) CNN for Gurgaon and (f) RNN for Gurgaon

(Purwani et al. 2022). It is noted that urban green spaces contribute a lot in lessening the heat exposure of a city (Jiang et al. 2024). Consequently, planned development of Gandhinagar has contributed for a mild UHI over the years. Evenly spaced buildings with urban green spaces within the built-up areas over the city has allowed easy passing of the cool and purified air within the bounds of the city (Damyano et al. 2024). The higher UHII during nighttime as compared to daytime could be accounted to the storage of larger amount of heat by the various urban structures (Memon et al. 2009). It is also quite relevant that due to high built-up areas, the summers will have a higher UHII than winters as is evidenced by the study of Pandey et al. 2023a, b. High nocturnal UHII of Dahegam can be attributed to the highly dense built-up areas which is more prominent in Dahegam than Gandhinagar, along with lesser green spaces (Song et al. 2020). Compared to Dahegam, built-up areas are not as dense in Kalol and hence the UHI effect is also lesser. However, they are denser when compared to Gandhinagar. Unlike other cities, UCI was not witnessed in Kalol as the intensity was mostly positive during the daytime of winters following a similar pattern in the nighttime too.

Bongaigaon has shown a slight increase in vegetation in the study period. This has come at the cost of barren land which is good for stabilization of LST in Bongaigaon. It is quite evident that the prevalence of healthy vegetation and green spaces within the city of Bongaigaon is highly important for the city to experience lesser UHI effect. Sun and Kafatos (2007) have also observed the negative association of LST with NDVI in warm seasons and vice-versa.

In Gurgaon, there is an increase in the vegetation class in the study area but it is in the vicinity of the city. Due to high-rise modern structures, the city has shown a high UHII, especially in the night. The occurrence of UCI in the days of winters can be accounted to the shades caused by the tall buildings thus making direct sunlight difficult to reach the land surface keeping LST low (Sun et al. 2024).

In the manuscript, the primary focus is to investigate the UHI effect in the study regions. If UHI value is found to be negative, then that it is considered as Urban Cool Island (UCI). When UHI values are found to be positive, then their magnitudes are compared. A city with higher positive UHI value is said to have a stronger Urban Heat Island Intensity (UHII). It may also be noted that the LST modeling of all the selected regions showed reasonably good performance, highlighting the potential of neural network-based models in capturing the association of LST with spectral indices and LULC Classes. The performance at the Gurgaon study region was better via both the models when compared to the other two study regions. Overall, RNN proved to be the better ML model than CNN in terms of R^2 . Such estimation of LST based on LULC information and the identification of seasonal UHI effects may be a key to a proper Urban Planning. It may be noted that the accuracy of the modeling approach adopted in this study is dependent on the accuracy/quality of the

satellite images which may get affected by cloud cover. Moreover, the revisit time of the satellites affect the frequency of data availability. For future LST projection, future land use information may be determined from cellular-automata based or random forest based approaches.

5 Summary and Conclusions

The findings of this study throw light on the occurrence of UHI/UCI effect in five Indian cities of various size, climate and stage of urban development during Summer and Winter seasons across 5 years (2006, 2010, 2014, 2018 and 2022). It was noted that UHI was experienced in all the five cities during summers whereas UCI was observed only in Bongaigaon even in summers. However, all the five cities have shown UCI mostly during the days of the winters at many a times over the five considered years. LSTs were higher in the cities mostly for both day and night and especially for summers. All the cities, except Kalol, have mostly shown an UCI during the winter days which can be accounted to the building shades making the LST lesser. It is evident from the highly built-up land of Gurgaon; the city has experienced a strong UHI over the years. Most of the UHI studies focus on the larger cities which makes the same unseen for smaller cities like Dahegam, Kalol and Bongaigaon which can also be a prey of UHI. Interestingly, the thickly built-up Dahegam and Kalol mostly had a higher T_u , T_{nu} and UHII values when compared to the nearby capital city Gandhinagar which has spacious buildings with small green spaces within. Hence growth of the city in a planned manner can also save even larger cities from a high UHI effect and an unplanned growth can lead to a high UHI effect even in smaller cities. Bongaigaon on the other hand has scattered built-up areas and a good vegetation even within the city, for which the city experienced UCI even during summers. Thus, in this study, an examination of the UHI/UCI effect across different cities with various climatic types and stages of urban development indicates that greening is the prime requirement in lessening the effect of UHI. Thus, growth of the cities should be such that the built-up areas should not be dense and should ideally have green spaces within.

Further, to fulfil the second objective of the study, LST was modelled for the selected cities from the observed spectral indices and observed LST data of previous mentioned years (2006, 2010, 2014, 2018 and 2022). It was observed that both the network based ML models, CNN and RNN, performed reasonably well but RNN proved to be better.

This study utilizes satellite data products from MODIS which have a coarser resolution compared to other satellite data products like Landsat- 8/9 or Sentinel- 2; this contributes to a limitation of this study in terms of the spatial LULC details that may be captured. In addition to the spectral indices used in this study, urban morphological factors such as, building shades, building density and urban green spaces

also play a pivotal role in altering the regional LST. If such detailed information is available, these may be incorporated as inputs for determining LST and UHI effects in future studies. Moreover, with the change of climate towards adversity, the prediction of future LST and UHI could be essential for

ensuring better preparedness. Future LULC projection may be attempted through advanced ML algorithms such as cellular automata or random forests for investigating future LST and UHI effect in all the growing cities where large urban sprawl is expected.

Appendix A. LULC confusion matrix, LST variation per LULC, UHII of the Cities and Train Plots of ML Analysis

Table 3 Confusion matrix for the validation of LULC of Gandhinagar district study area

LULC Class	Water Body	Vegetation	Barren Land	Agricultural & Fallow	Built-up Area	Total	User Accuracy	Kappa
Water Body	5	1	0	0	0	6	0.83	-
Vegetation	0	8	0	1	0	9	0.89	-
Barren Land	0	0	9	0	2	11	0.82	-
Agricultural & Fallow	3	0	3	89	1	96	0.93	-
Built-up Area	0	1	2	1	24	28	0.86	-
Total	8	10	14	91	27	150	-	-
Producer Accuracy	0.63	0.8	0.64	0.98	0.89	-	0.9*	-
Kappa	-	-	-	-	-	-	-	0.82**

*Overall Accuracy = 0.9, **Kappa Coefficient = 0.82

Table 4 Confusion matrix for the validation of LULC of Bongaigaon and surroundings study area

LULC Class	Water Body	Vegetation	Built-up Area	Agricultural & Fallow	Barren Land	Total	User Accuracy	Kappa
Water Body	8	0	0	1	0	9	0.89	-
Vegetation	0	13	0	0	1	14	0.93	-
Built-up Area	0	0	8	2	0	10	0.80	-
Agricultural & Fallow	0	1	0	28	0	29	0.97	-
Barren Land	1	0	0	0	7	8	0.88	-
Total	9	14	8	31	8	70	0.00	-
Producer Accuracy	0.89	0.93	1.00	0.90	0.88	0.00	0.91*	-
Kappa	-	-	-	-	-	-	-	0.88**

*Overall Accuracy = 0.91, **Kappa Coefficient = 0.88

Table 5 Confusion Matrix for the validation of LULC of Gurgaon Administrative Division Study Area

LULC Class	Vegetation	Built-up Area	Agricultural & Fallow	Total	User Accuracy	Kappa
Vegetation	7	0	0	7	1.00	-
Built-up Area	2	9	0	11	0.82	-
Agricultural & Fallow	3	0	79	82	0.96	-
Total	12	9	79	100	0.00	-
Producer Accuracy	0.58	1.00	1.00	0.00	0.95*	-
Kappa	-	-	-	-	-	0.85**

*Overall Accuracy = 0.95, **Kappa Coefficient = 0.85

Table 6 LST for every LULC category

Study Area	LULC Class	2006		2010		2014		2018		2022	
		Summer		Winter		Summer		Winter		Summer	
		Day	Night								
Gandhi nagar	Water Body	41.07	18.7	27.99	10.19	43.29	19.56	28.9	11.57	39.54	18.43
	Vegetation	39.78	17.64	26.46	9.16	40.22	18.29	26.25	11.04	37.79	18.06
	Built-up Area	40.79	18.43	28.13	10.11	42.29	19.25	29.41	11.17	43.42	18.28
Agricultural and Fallow	Agricultural and Fallow	41.48	18.65	28.02	10.03	42.7	19.63	28.71	11.43	39.54	18.31
Barren Land	Barren Land	41.73	18.99	28.23	10.24	44.52	19.95	28.89	11.6	40.2	18.7
Bongaigaon	Water Body	28.27	18.49	21.98	12.27	28.46	18.55	21.54	12.05	27.79	18.33
	Vegetation	25.43	18.55	22.66	13.65	25.21	18.03	22.07	12.26	25.77	17.82
	Built-up Area	27.55	18.27	22.44	13.23	27.43	18.99	21.31	12.74	27.06	19.24
	Agricultural and Fallow	28.6	18.59	22.64	13.72	27.39	18.32	20.65	12.34	28.08	18.31
	Barren Land	28.62	18.54	22.65	13.63	28.33	18.33	21.09	12.28	28.11	18.28
Gurgaon	Vegetation	31.87	16.97	19.08	10.01	32.11	17.74	19.18	9.18	33.21	16.6
	Built-up Area	33.45	19.09	19.02	10.69	33.15	20.2	18.43	11.17	36.3	17.27
	Agricultural and Fallow	31.09	14.38	19.05	8.24	32.08	15.23	19.39	7.68	28.95	15.21

Table 7 UHII for Gandhinagar

Season	Date	Time	T _u	T _{nu}	UHII
Summer	30–03–2006	Day	41.29	41.27	0.01
Summer	13–03–2010	Day	44.49	44.39	0.10
Summer	13–03–2014	Day	36.55	36.35	0.21
Summer	30–03–2018	Day	45.51	44.74	0.77
Summer	12–03–2022	Day	40.75	40.58	0.17
Summer	30–03–2006	Night	20.56	19.30	1.26
Summer	13–03–2010	Night	22.33	20.53	1.80
Summer	13–03–2014	Night	20.61	19.55	1.06
Summer	30–03–2018	Night	23.48	21.93	1.54
Summer	12–03–2022	Night	22.18	20.91	1.27
Winter	30–12–2006	Day	28.05	27.97	0.08
Winter	14–12–2010	Day	28.02	28.74	−0.72
Winter	14–12–2014	Day	27.97	28.37	−0.40
Winter	30–12–2018	Day	27.11	27.25	−0.14
Winter	30–12–2022	Day	28.63	28.40	0.23
Winter	30–12–2006	Night	14.40	13.44	0.96
Winter	14–12–2010	Night	12.96	11.68	1.28
Winter	14–12–2014	Night	11.77	10.58	1.19
Winter	30–12–2018	Night	13.20	11.74	1.46
Winter	30–12–2022	Night	16.69	15.50	1.19

Table 8 UHII for Dahegam

Season	Date	Time	T _u	T _{nu}	UHII
Summer	30–03–2006	Day	41.74	42.08	−0.34
Summer	13–03–2010	Day	46.54	44.90	1.65
Summer	13–03–2014	Day	47.89	46.12	1.77
Summer	30–03–2018	Day	47.48	45.83	1.64
Summer	12–03–2022	Day	42.89	40.62	2.27
Summer	30–03–2006	Night	19.00	18.29	0.71
Summer	13–03–2010	Night	19.74	19.28	0.46
Summer	13–03–2014	Night	18.62	17.88	0.74
Summer	30–03–2018	Night	21.78	20.78	1.00
Summer	12–03–2022	Night	21.12	20.40	0.73
Winter	30–12–2006	Day	27.72	27.97	−0.25
Winter	14–12–2010	Day	29.14	29.15	0.00
Winter	14–12–2014	Day	29.22	29.25	−0.03
Winter	30–12–2018	Day	25.16	25.89	−0.74
Winter	30–12–2022	Day	27.14	27.48	−0.33
Winter	30–12–2006	Night	13.35	12.95	0.40
Winter	14–12–2010	Night	12.08	11.28	0.80
Winter	14–12–2014	Night	10.33	9.58	0.75
Winter	30–12–2018	Night	11.36	10.92	0.44
Winter	30–12–2022	Night	14.56	14.09	0.47

Table 9 UHII for Kalol

Season	Date	Time	T _u	T _{nu}	UHII
Summer	30–03–2006	Day	42.20	41.91	0.30
Summer	13–03–2010	Day	44.00	43.33	0.67
Summer	13–03–2014	Day	36.84	36.01	0.82
Summer	30–03–2018	Day	46.19	45.49	0.70
Summer	12–03–2022	Day	40.64	39.67	0.97
Summer	30–03–2006	Night	20.09	19.07	1.02
Summer	13–03–2010	Night	21.20	20.09	1.12
Summer	13–03–2014	Night	19.93	18.69	1.24
Summer	30–03–2018	Night	22.38	21.73	0.64
Summer	12–03–2022	Night	22.80	21.18	1.62
Winter	30–12–2006	Day	28.43	27.85	0.58
Winter	14–12–2010	Day	28.95	28.83	0.12
Winter	14–12–2014	Day	27.77	27.79	−0.02
Winter	30–12–2018	Day	27.29	26.76	0.53
Winter	30–12–2022	Day	29.11	28.28	0.84
Winter	30–12–2006	Night	13.86	13.22	0.65
Winter	14–12–2010	Night	12.43	12.40	0.03
Winter	14–12–2014	Night	11.50	10.77	0.72
Winter	30–12–2018	Night	12.14	11.83	0.31
Winter	30–12–2022	Night	16.25	15.07	1.18

Table 10 UHII for Bongaigaon

Season	Date	Time	T _u	T _{nu}	UHII
Summer	30–03–2006	Day	29.23	29.23	0.00
Summer	13–03–2010	Day	23.05	23.05	0.00
Summer	13–03–2014	Day	29.85	30.28	– 0.43
Summer	30–03–2018	Day	28.78	29.34	– 0.55
Summer	12–03–2022	Day	30.00	30.57	– 0.56
Summer	30–03–2006	Night	18.54	18.77	– 0.24
Summer	13–03–2010	Night	17.38	16.61	0.77
Summer	13–03–2014	Night	15.19	14.15	1.04
Summer	30–03–2018	Night	18.34	17.98	0.36
Summer	12–03–2022	Night	21.53	20.50	1.03
Winter	30–12–2006	Day	22.64	22.47	0.17
Winter	14–12–2010	Day	20.09	20.09	0.00
Winter	14–12–2014	Day	23.37	23.70	– 0.33
Winter	30–12–2018	Day	24.34	25.20	– 0.86
Winter	30–12–2022	Day	23.25	23.95	– 0.70
Winter	30–12–2006	Night	13.72	13.79	– 0.07
Winter	14–12–2010	Night	12.78	12.30	0.48
Winter	14–12–2014	Night	13.25	12.07	1.18
Winter	30–12–2018	Night	15.10	14.05	1.05
Winter	30–12–2022	Night	17.08	16.38	0.70

Table 11 UHII for Gurgaon

Season	Date	Time	T _u	T _{nu}	UHII
Summer	30–03–2006	Day	33.55	31.78	1.77
Summer	13–03–2010	Day	33.13	32.76	0.37
Summer	13–03–2014	Day	36.24	34.54	1.70
Summer	30–03–2018	Day	34.81	33.56	1.25
Summer	12–03–2022	Day	32.32	31.72	0.60
Summer	30–03–2006	Night	16.00	12.24	3.76
Summer	13–03–2010	Night	18.81	15.11	3.70
Summer	13–03–2014	Night	17.27	15.71	1.56
Summer	30–03–2018	Night	20.94	17.59	3.35
Summer	12–03–2022	Night	22.13	18.84	3.29
Winter	30–12–2006	Day	23.48	23.60	– 0.12
Winter	14–12–2010	Day	21.67	22.66	– 0.99
Winter	14–12–2014	Day	17.58	18.74	– 1.16
Winter	30–12–2018	Day	20.46	20.75	– 0.29
Winter	30–12–2022	Day	20.17	20.33	– 0.17
Winter	30–12–2006	Night	5.23	4.25	0.98
Winter	14–12–2010	Night	10.24	7.54	2.70
Winter	14–12–2014	Night	11.77	9.81	1.96
Winter	30–12–2018	Night	10.14	7.52	2.62
Winter	30–12–2022	Night	12.12	9.81	2.32

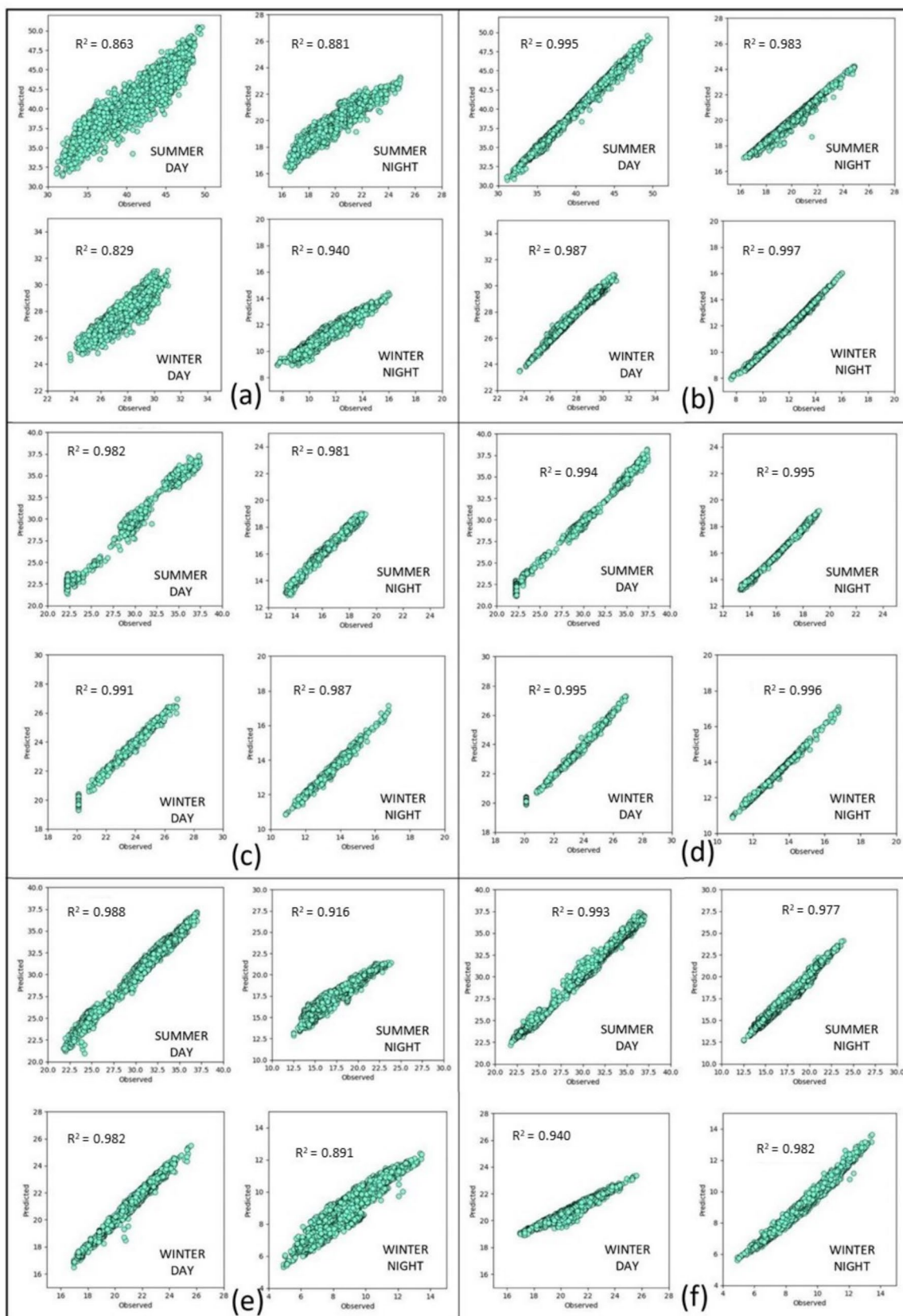


Fig. 11 Train Plots of (a) CNN for Gandhinagar, (b) RNN for Gandhinagar, (c) CNN for Bongaigaon (d) RNN for Bongaigaon, (e) CNN for Gurgaon and (f) RNN for Gurgaon

Table 12 Summary of R^2 values for both CNN and RNN

Study Area	CNN								RNN							
	Summer				Winter				Summer				Winter			
	Day		Night		Day		Night		Day		Night		Day		Night	
	Train	Test	Train	Test												
Gandhinagar	0.863	0.828	0.881	0.776	0.829	0.850	0.940	0.851	0.995	0.967	0.983	0.98	0.987	0.979	0.997	0.967
Bongaigaon	0.982	0.738	0.981	0.938	0.991	0.936	0.987	0.944	0.994	0.9	0.995	0.961	0.995	0.969	0.996	0.915
Gurgaon	0.988	0.911	0.916	0.940	0.982	0.906	0.891	0.891	0.993	0.904	0.977	0.978	0.940	0.811	0.982	0.97

Acknowledgements We acknowledge partial support from Ministry of Earth Science (MoES), Government of India through the project MoES/PAMC/H & C/124/2019-PC-II. We acknowledge NASA for provision of the MODIS products through the website of LAADS DAAC (<https://ladsweb.modaps.eosdis.nasa.gov/>) which was helpful for the study. We acknowledge Survey of India, Ministry of Science and Technology for provision of the various shapefiles at various administrative levels which were useful in denoting the area of interests particularly and these were obtained from their website (<https://onlinemaps.surveynofindia.gov.in/>).

Author contribution NIRUP SUNDAR MANDAL: Methodology; formal analysis; investigation; visualization; writing – original draft; data curation. KIRONMALA CHANDA: Conceptualization; methodology; supervision; writing – review and editing.

Data availability Data is derived from the open sources which are acknowledged in the manuscript.

Declarations

Competing Interests The authors declare no competing interests.

References

- Alademomi AS, Okolie CJ, Daramola OE et al (2022) The interrelationship between LST, NDVI, NDBI, and land cover change in a section of Lagos metropolis, Nigeria. *Appl Geomatics* 14:299–314. <https://doi.org/10.1007/s12518-022-00434-2>
- Almouctar MAS, Wu Y, Zhao F, Qin C (2024) Drought analysis using normalized difference vegetation index and land surface temperature over Niamey region, the southwestern of the Niger between 2013 and 2019. *J Hydrol Reg Stud* 52:101689. <https://doi.org/10.1016/j.ejrh.2024.101689>
- Arpit D, Kanuparthi B, Kerg G, Ke NR, Mitliagkas I, Bengio Y (2018) h-detach: modifying the LSTM gradient towards better optimization. arXiv preprint arXiv:1810.03023
- Bahadur TK (2009) Urbanization in North-East India. Mittal Publications
- Bala R, Prasad R, Yadav VP (2020) Thermal sharpening of MODIS land surface temperature using statistical downscaling technique in urban areas. *Theor Appl Climatol* 141:935–946. <https://doi.org/10.1007/s00704-020-03253-w>
- Becker F, Li ZL (1990) Towards a local split window method over land surfaces. *Int J Remote Sens* 11:369. <https://doi.org/10.1080/01431169008955028>
- Bochenek B, Ustrnul Z (2022) Machine Learning in Weather Prediction and Climate Analyses—Applications and Perspectives. *Atmosphere* (Basel) 13:1–16. <https://doi.org/10.3390/atmos13020180>
- Borah S, Sarma K (2025) Temporal assessment of land surface temperature and urban heat island temporal assessment of land surface temperature and urban heat island effect in Guwahati City : A geospatial analysis. *Eco Env Cons* 31:S26–S33. <https://doi.org/10.53550/EEC.2025.v31i01s.006>
- Bounoua I, Saidi Y, Yaagoubi R, Bouziani M (2024) Deep learning approaches for water stress forecasting in arboriculture using time series of remote sensing images: Comparative study between ConvLSTM and CNN-LSTM models. *Technologies* 12:77. <https://doi.org/10.3390/technologies12060077>
- Cersosimo A, Serio C, Masiello G (2020) TROPOMI NO₂ tropospheric column data: Regridding to 1 km grid-resolution and assessment of their consistency with in situ surface observations. *Remote Sens* 12:2212. <https://doi.org/10.3390/rs12142212>
- Chen S, Yu Z, Liu M et al (2021) Trends of the contributions of biophysical (climate) and socioeconomic elements to regional heat islands. *Sci Rep* 11:12696. <https://doi.org/10.1038/s41598-021-92271-3>
- Chowdhury MS (2023) GIS based method for mapping actual LULC by combining seasonal LULCs. *MethodsX* 11:102472. <https://doi.org/10.1016/j.mex.2023.102472>
- Damyanovic D, Gabor A, Grimm K, Reinwald F (2024) “Cool public spaces for the cities”: a climate-fit approach to the urban design of public streetscapes and squares—a vital contribution to climate-responsive cities. In: Research handbook on urban design. Edward Elgar Publishing, pp 331–348
- Dao MS, Zettsu K (2018) Complex Event Analysis of Urban Environmental Data based on Deep CNN of Spatiotemporal Raster Images. *Proc - 2018 IEEE Int Conf Big Data. Big Data* 2018:2160–2169. <https://doi.org/10.1109/BigData.2018.8621916>
- de Moura CN, Seibert J, Detzel DHM (2022) Evaluating the long short-term memory (LSTM) network for discharge prediction under changing climate conditions. *Hydrol Res* 53:657–667. <https://doi.org/10.2166/NH.2022.044>
- Debsarma C, Sahu P, Kalubarme MH (2023) Influence assessment of urban expansion on groundwater level fluctuations in Gandhinagar, Gujarat India. *Environ Monit Assess* 195:1123. <https://doi.org/10.1007/s10661-023-11709-5>
- Diek S, Fornallaz F, Schaeppman ME, de Jong R (2017) Barest pixel composite for agricultural areas using landsat time series. *Remote Sens* 9:1245. <https://doi.org/10.3390/rs9121245>
- Equere V, Mirzaei PA, Riffat S, Wang Y (2021) Integration of topographical aspect of city terrains to predict the spatial distribution of urban heat island using GIS and ANN. *Sustain Cities Soc* 69:102825. <https://doi.org/10.1016/j.scs.2021.102825>

- Feng Y, Li H, Tong X et al (2018) Projection of land surface temperature considering the effects of future land change in the Taihu Lake Basin of China. *Glob Planet Change* 167:24–34. <https://doi.org/10.1016/j.gloplacha.2018.05.007>
- Friedl M, Sulla-Menashe D (2019) MCD12Q1 MODIS/Terra+ aqua land cover type yearly L3 global 500m SIN grid V006
- Gallo KP, Flesch TK (1989) Large-Area Crop Monitoring with the NOAA AVHRR: Estimating the Silking Stage of Corn Development. *Remote Sens Environ* 27(1):73–80
- Gers FA, Schmidhuber J, Cummins F (1999) Continual prediction using LSTM with forget gates. In: Neural nets WIRN vietri-99: proceedings of the 11th Italian workshop on neural nets, Vietri Sul Mare, Salerno, Italy, 20–22 May 1999. Springer London, pp 133–138
- Gholamalinezhad H, Khosravi H (2020) Pooling methods in deep neural networks, a review. arXiv preprint arXiv:2009.07485
- Gohain KJ, Goswami A, Mohammad P, Kumar S (2023) Modelling relationship between land use land cover changes, land surface temperature and urban heat island in Indore city of central India. *Theor Appl Climatol* 151:1981–2000. <https://doi.org/10.1007/s00704-023-04371-x>
- Gu J, Wang Z, Kuen J et al (2018) Recent advances in convolutional neural networks. *Pattern Recognit* 77:354–377. <https://doi.org/10.1016/j.patcog.2017.10.013>
- Guha S, Govil H (2021) An assessment on the relationship between land surface temperature and normalized difference vegetation index. *Environ Dev Sustain* 23:1944–1963. <https://doi.org/10.1007/s10668-020-00657-6>
- Guha S, Govil H (2022) Annual assessment on the relationship between land surface temperature and six remote sensing indices using landsat data from 1988 to 2019. *Geocarto Int* 37:4292–4311. <https://doi.org/10.1080/10106049.2021.1886339>
- Guo Y, Zhang L, He Y et al (2024) LSTM time series NDVI prediction method incorporating climate elements: A case study of Yellow River Basin China. *J Hydrol* 629:130518. <https://doi.org/10.1016/j.jhydrol.2023.130518>
- Jain RK, Jain K, Ali SR (2017) Remote sensing enabled urban growth analysis for Gurgaon from 1995 to 2015. *Adv Comput Sci Technol* 10:1745–1757
- Jandaghian Z, Colombo A (2024) The role of water bodies in climate regulation: insights from recent studies on urban heat island mitigation. *Build* 14(9):2945
- Jiang L, Xie M, Chen B et al (2024) Key areas and measures to mitigate heat exposure risk in highly urbanized city: A case study of Beijing China. *Urban Clim* 53:101748. <https://doi.org/10.1016/j.uclim.2023.101748>
- Joshi K, Kumari M, Mishra VN et al (2025) Geoinformatics based evaluation of heat mitigation strategies through urban green spaces in a rapidly growing city of India: implications for urban resilience. *Theor Appl Climatol* 156:1–24. <https://doi.org/10.1007/s00704-025-05411-4>
- Kafy AA, Faisal AA, Shuvo RM et al (2021) Remote sensing approach to simulate the land use/land cover and seasonal land surface temperature change using machine learning algorithms in a fast-growing megacity of Bangladesh. *Remote Sens Appl Soc Environ* 21:100463. <https://doi.org/10.1016/j.rsase.2020.100463>
- Kaplan G, Avdan U, Avdan ZY (2018) Urban heat island analysis using the landsat 8 satellite data: a case study in Skopje, Macedonia. *Proc MDPI* 2(7):358
- Kartal S, Sekertekin A (2022) Prediction of MODIS land surface temperature using new hybrid models based on spatial interpolation techniques and deep learning models. *Environ Sci Pollut Res* 29:67115–67134. <https://doi.org/10.1007/s11356-022-20572-9>
- Kawamura M (1996) Relation between social and environmental conditions in colombo, sri lanka and the urban index estimated by satellite remote sensing data. *Int Arch Photogramm Remote Sens* 7:321–326
- Khamchiangta D, Dhakal S (2020) Time series analysis of land use and land cover changes related to urban heat island intensity: Case of Bangkok Metropolitan Area in Thailand. *J Urban Manag* 9:383–395. <https://doi.org/10.1016/j.jum.2020.09.001>
- Khan A, Khan HH, Khan A (2024) Time-series analysis of remotely sensed biophysical parameters and their effects on land surface temperature (LST): a case study of Aligarh region, India. *Acta Geophys* 72:2887–2905. <https://doi.org/10.1007/s11600-023-01252-9>
- Konwar P (2024) The cost of unplanned infrastructure development in Assam: environmental and social impact of roads and bridges
- Liang D, Zuo Y, Huang L et al (2015) Evaluation of the consistency of MODIS land cover product (MCD12Q1) based on Chinese 30 m GlobeLand30 datasets: A case study in Anhui Province, China. *ISPRS Int J Geo-Information* 4:2519–2541. <https://doi.org/10.3390/ijgi4042519>
- Liu B, Xie Z, Qin P et al (2021) Increases in anthropogenic heat release from energy consumption lead to more frequent extreme heat events in urban cities. *Adv Atmos Sci* 38:430–445. <https://doi.org/10.1007/s00376-020-0139-y>
- Liu FA, Wang X, Sun F et al (2022) Correction of overestimation in observed land surface temperatures based on machine learning models. *J Clim* 35(16):5359–5377. <https://doi.org/10.1175/JCLI-D-21>
- Martins TAL, Adolphe L, Bonhomme M et al (2016) Impact of Urban Cool Island measures on outdoor climate and pedestrian comfort: Simulations for a new district of Toulouse, France. *Sustain Cities Soc* 26:9–26. <https://doi.org/10.1016/j.scs.2016.05.003>
- Mathew A, Khandelwal S, Kaul N (2017) Investigating spatial and seasonal variations of urban heat island effect over Jaipur city and its relationship with vegetation, urbanization and elevation parameters. *Sustain Cities Soc* 35:157–177. <https://doi.org/10.1016/j.scs.2017.07.013>
- Memon RA, Leung DYC, Liu CH (2009) An investigation of urban heat island intensity (UHII) as an indicator of urban heating. *Atmos Res* 94:491–500. <https://doi.org/10.1016/j.atmosres.2009.07.006>
- Mohammad P, Goswami A (2021) A spatio-temporal assessment and prediction of surface urban heat island intensity using multiple linear regression techniques over Ahmedabad City, Gujarat. *J Indian Soc Remote Sens* 49:1091–1108. <https://doi.org/10.1007/s12524-020-01299-x>
- Mohammad Harmay NS, Kim D, Choi M (2021) Urban heat island associated with land use/land cover and climate variations in Melbourne Australia. *Sustain Cities Soc* 69:102861. <https://doi.org/10.1016/j.scs.2021.102861>
- Muhammad R, Zhang W, Abbas Z et al (2022) Spatiotemporal change analysis and prediction of future land use and land cover changes using QGIS MOLUSCE plugin and remote sensing big data: A case study of Linyi China. *Land* 11:419. <https://doi.org/10.3390/land11030419>
- O'shea K, Nash R (2015) An introduction to convolutional neural networks. arXiv preprint arXiv:1511.08458
- Ouma YO, Omai L (2023) Flood susceptibility mapping using image-based 2D-CNN deep learning: Overview and case study application using multiparametric spatial data in data-scarce urban environments. *Int J Intell Syst* 2023:5672401. <https://doi.org/10.1155/2023/5672401>
- Pandey A, Mondal A, Guha S et al (2022) A seasonal investigation on land surface temperature and spectral indices in Imphal City, India. *J Landsc Ecol Republic* 15:1–18. <https://doi.org/10.2478/jlecol-2022-0015>
- Pandey A, Mondal A, Guha S et al (2023) Analysis of the variability in land surface temperature due to land use/land cover change for

- a sustainable urban planning. *J Landsc Ecol Republic* 16:20–35. <https://doi.org/10.2478/jlecol-2023-0015>
- Pandey A, Mondal A, Guha S et al (2023b) Analysis of spectral indices-based downscaled land surface temperature in a humid subtropical city. *Int J Image Data Fusion* 14:336–358. <https://doi.org/10.1080/19479832.2023.2252818>
- Pasi KG, Naik SR (2016) Effect of parameter variations on accuracy of convolutional neural network. In: 2016 international conference on computing, analytics and security trends (cast). IEEE, pp 398–403
- Patra PK, Behera D, Chetry V et al (2025) Geospatial analysis of unplanned urbanization: Impact on land surface temperature and habitat suitability in Cuttack India. *Discov Sustain* 6:118. <https://doi.org/10.1007/s43621-025-00920-8>
- Petrolli N (2013) The Normalized Difference Vegetation Index. Oxford University Press
- Phiphiphatphaisit S, Surinta O (2021) Deep feature extraction technique based on conv1d and lstm network for food image recognition. *Eng Appl Sci Res* 48:581–592. <https://doi.org/10.14456/easr.2021.60>
- Pulver A, Lyu S (2017) LSTM with working memory. In: 2017 international joint conference on neural networks (IJCNN). IEEE, pp 845–851
- Purswani E, Verma S, Jayakumar S et al (2022) Examining and predicting land use change dynamics in Gandhinagar district, Gujarat, India. *J Urban Manag* 11:82–96. <https://doi.org/10.1016/j.jum.2021.09.003>
- Raza D, Khushi M, Shu H et al (2024) CA-ANN based LULC prediction and influence assessment on LST-NDVI using multi-temporal satellite images. *Environ Earth Sci* 83:1–20. <https://doi.org/10.1007/s12665-024-11467-8>
- Rezaei Rad H, Rafeian M, Sozer H (2020) Evaluating the effects of increasing of building height on land surface temperature. *Int J Urban Manag Energy Sustain* 1:37–42. <https://doi.org/10.22034/ijumes.2019.01.01.002>
- Russakovsky O, Deng J, Su H et al (2015) ImageNet large scale visual recognition challenge. *Int J Comput vis* 115:211–252. <https://doi.org/10.1007/s11263-015-0816-y>
- Santhosh LG, Shilpa DN (2023) Assessment of LULC change dynamics and its relationship with LST and spectral indices in a rural area of Bengaluru district, Karnataka India. *Remote Sensing Applications: Society and Environment* 29:100886
- Sarif MO, Ranagalage M, Gupta RD, Murayama Y (2022) Monitoring urbanization induced surface urban cool island formation in a South Asian megacity: A case study of Bengaluru, India (1989–2019). *Front Ecol Evol* 10:901156. <https://doi.org/10.3389/fevo.2022.901156>
- Schlaerth HL, Silva SJ, Li Y, Li D (2023) Albedo as a competing warming effect of urban greening. *J Geophys Res Atmos* 128:1–14. <https://doi.org/10.1029/2023JD038764>
- Shahfahad, Kumari B, Tayyab M, Ahmed IA, Baig MRI, Khan MF, Rahman A (2020) Longitudinal study of land surface temperature (LST) using mono-and split-window algorithms and its relationship with NDVI and NDBI over selected metro cities of India. *Arab J Geosci* 13:1–19
- Song J, Chen W, Zhang J et al (2020) Effects of building density on land surface temperature in China: Spatial patterns and determinants. *Landsc Urban Plan* 198:103794. <https://doi.org/10.1016/j.landurbplan.2020.103794>
- Staudemeyer RC, Morris ER (2019) Understanding LSTM--a tutorial into long short-term memory recurrent neural networks. arXiv preprint arXiv:1909.09586
- Subzar Malik M, Prakash Shukla J, Mishra S (2019) Relationship of LST, NDBI and NDVI using Landsat-8 data in Kandaihimmat Watershed. Hoshangabad, India
- Sun H, Zhao X, Chen Y et al (2013) A new agricultural drought monitoring index combining MODIS NDWI and day-night land surface temperatures: A case study in China. *Int J Remote Sens* 34:8986–9001. <https://doi.org/10.1080/01431161.2013.860659>
- Sun T, Chen L, Sun R (2024) Cooling effects in urban communities: Parsing green spaces and building shadows. *Urban for Urban Green* 94:128264. <https://doi.org/10.1016/j.ufug.2024.128264>
- Sun D, Kafatos M (2007) Note on the NDVI-LST relationship and the use of temperature-related drought indices over North America. *Geophys Res Lett* 34. <https://doi.org/10.1029/2007GL031485>
- Sundermeyer M, Schlüter R, Ney H (2012) Lstm neural networks for language modeling. *Interspeech* 2012:194–197
- Tan KC, Lim HS, MatJafri MZ, Abdullah K (2012) A comparison of radiometric correction techniques in the evaluation of the relationship between LST and NDVI in Landsat imagery. *Environ Monit Assess* 184:3813–3829. <https://doi.org/10.1007/s10661-011-2226-0>
- Uddin S, Lu H (2024) Confirming the statistically significant superiority of tree-based machine learning algorithms over their counterparts for tabular data. *PLoS ONE* 19:1–12. <https://doi.org/10.1371/journal.pone.0301541>
- Varamesh S, MohtaramAnbaran S, Shirmohammadi B et al (2022) How do different land uses/covers contribute to land surface temperature and albedo? *Sustain* 14:16963. <https://doi.org/10.3390/su142416963>
- Venkatesan R, Li B (2017) Convolutional neural networks in visual computing: a concise guide. CRC Press
- Vermote E (2015) MOD09A1 MODIS/terra surface reflectance 8-day L3 global 500m SIN grid V006
- Wan Z, Dozier J (1996) A generalized split-window algorithm for retrieving land-surface temperature from space. *IEEE Trans Geosci Remote Sens* 34(4):892–905
- Wan Z, Hook S, Hulley G (2021) MODIS/terra land surface temperature/emissivity 8-day L3 global 1km SIN grid V061
- Wong NH, Yu C (2005) Study of green areas and urban heat island in a tropical city. *Habitat Int* 29:547–558. <https://doi.org/10.1016/j.habitatint.2004.04.008>
- Xu H (2005) A study on information extraction of water body with the modified normalized difference water index (MNDWI). *Natl Rem Sens Bull* 5:589–595
- Xu H, Li C, Hu Y et al (2024) Urban Climate Spatiotemporal evolution and influencing factors of surface urban heat island footprint across different-sized cities. *Urban Clim* 54:101852. <https://doi.org/10.1016/j.ulclim.2024.101852>
- Xue J, Zhang X, Chen S et al (2024) Quantifying the agreement and accuracy characteristics of four satellite-based LULC products for cropland classification in China. *J Integr Agric* 23:283–297. <https://doi.org/10.1016/j.jia.2023.06.005>
- Yang L, Qian F, Song DX, Zheng KJ (2016) Research on urban heat-island effect. *Procedia Eng* 169:11–18
- Zeng Y, Huang W, Zhan F et al (2010) Study on the urban heat island effects and its relationship with surface biophysical characteristics using MODIS imagers. *Geo-Spatial Inf Sci* 13:1–7. <https://doi.org/10.1007/s11806-010-0204-2>
- Zha Y, Gao J, Ni S (2003) Use of normalized difference built-up index in automatically mapping urban areas from TM imagery. *Int J Remote Sens* 24:583–594. <https://doi.org/10.1080/01431160304987>
- Zhang M, Al Kafy A, Xiao P et al (2023) Impact of urban expansion on land surface temperature and carbon emissions using machine learning algorithms in Wuhan China. *Urban Clim* 47:101347. <https://doi.org/10.1016/j.ulclim.2022.101347>
- Zhang S, Yang Y, Xie K et al (2024) Spatial-temporal siamese convolutional neural network for subsurface temperature reconstruction. *IEEE Trans Geosci Remote Sens* 62:1–16. <https://doi.org/10.1109/TGRS.2023.3348653>

- Zheng L, Zhao Y, Wang S, Wang J, Tian Q (2016) Good practice in CNN feature transfer. arXiv preprint arXiv:1604.00133
- Zhou B, Rybski D, Kropf JP (2013) On the statistics of urban heat island intensity. *Geophys Res Lett* 40:5486–5491. <https://doi.org/10.1002/2013GL057320>
- Zou Z, Yan C, Yu L et al (2021) Impacts of land use/ land cover types on interactions between urban heat island effects and heat waves. *Build Environ* 204:108138. <https://doi.org/10.1016/j.buildenv.2021.108138>

Publisher's Note Springer Nature remains neutral with regard to jurisdictional claims in published maps and institutional affiliations.

Springer Nature or its licensor (e.g. a society or other partner) holds exclusive rights to this article under a publishing agreement with the author(s) or other rightsholder(s); author self-archiving of the accepted manuscript version of this article is solely governed by the terms of such publishing agreement and applicable law.